

[Handwritten signature]

MAR 12 1982

C2



Aeroballistics Range Photopyrometry

P. H. Dugger, C. P. Enis, and R. E. Hendrix
ARO, Inc.

February 1982

Final Report for Period October 1976 — September 1978

Approved for public release; distribution unlimited.

Property of U.S. Air Force
AEDC-TR-82-1
F46660-81-0-0004

**ARNOLD ENGINEERING DEVELOPMENT CENTER
ARNOLD AIR FORCE STATION, TENNESSEE
AIR FORCE SYSTEMS COMMAND
UNITED STATES AIR FORCE**

NOTICES

When U. S. Government drawings, specifications, or other data are used for any purpose other than a definitely related Government procurement operation, the Government thereby incurs no responsibility nor any obligation whatsoever, and the fact that the government may have formulated, furnished, or in any way supplied the said drawings, specifications, or other data, is not to be regarded by implication or otherwise, or in any manner licensing the holder or any other person or corporation, or conveying any rights or permission to manufacture, use, or sell any patented invention that may in any way be related thereto.

Qualified users may obtain copies of this report from the Defense Technical Information Center.

References to named commercial products in this report are not to be considered in any sense as an endorsement of the product by the United States Air Force or the Government.

This report has been reviewed by the Office of Public Affairs (PA) and is releasable to the National Technical Information Service (NTIS). At NTIS, it will be available to the general public, including foreign nations.

APPROVAL STATEMENT

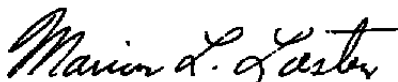
This report has been reviewed and approved.



MARSHALL K. KINGERY
Directorate of Technology
Deputy of Technology

Approved for publication:

FOR THE COMMANDER



MARION L. LASTER
Director of Technology
Deputy for Operations

UNCLASSIFIED

SECURITY CLASSIFICATION OF THIS PAGE (When Data Entered)

REPORT DOCUMENTATION PAGE		READ INSTRUCTIONS BEFORE COMPLETING FORM												
1. REPORT NUMBER AEDC-TR-79-34	2. GOVT ACCESSION NO.	3. RECIPIENT'S CATALOG NUMBER												
4. TITLE (and Subtitle) AEROBALLISTICS RANGE PHOTOPYROMETRY		5. TYPE OF REPORT & PERIOD COVERED Final Report - October 1976 - September 1978												
		6. PERFORMING ORG. REPORT NUMBER												
7. AUTHOR(s) P. H. Dugger, C. P. Enis, and R. E. Hendrix, ARO, Inc., a Sverdrup Corporation Company		8. CONTRACT OR GRANT NUMBER(s)												
9. PERFORMING ORGANIZATION NAME AND ADDRESS Arnold Engineering Development Center/DOTR Air Force Systems Command Arnold Air Force Station, Tennessee 37389		10. PROGRAM ELEMENT, PROJECT, TASK AREA & WORK UNIT NUMBERS Program Element 65807F												
11. CONTROLLING OFFICE NAME AND ADDRESS Arnold Engineering Development Center/DOS Air Force Systems Command Arnold Air Force Station, Tennessee 37389		12. REPORT DATE February 1982												
14. MONITORING AGENCY NAME & ADDRESS (if different from Controlling Office)		13. NUMBER OF PAGES 49												
		15. SECURITY CLASS. (of this report) UNCLASSIFIED												
		15a. DECLASSIFICATION/DOWNGRADING SCHEDULE N/A												
16. DISTRIBUTION STATEMENT (of this Report) Approved for public release; distribution unlimited.														
17. DISTRIBUTION STATEMENT (of the abstract entered in Block 20, if different from Report)														
18. SUPPLEMENTARY NOTES Available in Defense Technical Information Center (DTIC).														
19. KEY WORDS (Continue on reverse side if necessary and identify by block number) <table border="0"> <tr> <td>optical pyrometers</td> <td>ranges</td> <td>measurement</td> </tr> <tr> <td>measuring instruments</td> <td>image intensifiers</td> <td>materials</td> </tr> <tr> <td>photography</td> <td>cameras</td> <td>reentry vehicles</td> </tr> <tr> <td>aeroballistics</td> <td>temperature</td> <td></td> </tr> </table>			optical pyrometers	ranges	measurement	measuring instruments	image intensifiers	materials	photography	cameras	reentry vehicles	aeroballistics	temperature	
optical pyrometers	ranges	measurement												
measuring instruments	image intensifiers	materials												
photography	cameras	reentry vehicles												
aeroballistics	temperature													
20. ABSTRACT (Continue on reverse side if necessary and identify by block number) <p>The development of photopyrometry systems employing state-of-the-art image intensifiers has extended the lower limit for in-flight nosetip surface temperature measurements on track-guided models in the AEDC Hyperballistic Range (G) to 1,250 K. Two recently developed types of photopyrometers are used to span the 1,250- to 4,000-K temperature measurement range during reentry materials evaluation testing. Measurement uncertainty associated</p>														

UNCLASSIFIED

UNCLASSIFIED

SECURITY CLASSIFICATION OF THIS PAGE(When Data Entered)

20. ABSTRACT (Continued).

solely with the photopyrometry systems is ± 130 K or better for measurement of any temperature within this measurement range.

UNCLASSIFIED

SECURITY CLASSIFICATION OF THIS PAGE(When Data Entered)

PREFACE

The work reported herein was conducted by the Arnold Engineering Development Center (AEDC), Air Force Systems Command (AFSC), under Program Element 65807F. The results were obtained by ARO, Inc., AEDC Division (a Sverdrup Corporation Company), operating contractor for the AEDC, AFSC, Arnold Air Force Station, Tennessee. The research was done under ARO Project Nos. V32I-A6A and V32S-P6A, and the manuscript was submitted for publication on April 11, 1979.

CONTENTS

	<u>Page</u>
1.0 INTRODUCTION	5
2.0 TRACK G SYSTEMS	
2.1 System Description	6
2.2 Calibration	7
3.0 DATA ACQUISITION AND REDUCTION	8
4.0 TYPICAL RESULTS	9
5.0 CONDITIONS AND ASSUMPTIONS	9
6.0 MEASUREMENT UNCERTAINTY	
6.1 System-Related Error Sources	10
6.2 Test-Related Error Sources	13
6.3 Summary of Temperature Measurement Uncertainty	16
7.0 CONCLUDING REMARKS	16
REFERENCES	17

ILLUSTRATIONS

Figure

1. Track Photopyrometer Arrangement	19
2. Typical Photopyrometer Calibration Photographs	20
3. Data Acquisition and Reduction	21
4. Photopyrometer Calibration Curves	22
5. Self-Luminosity Photograph of Track G Model—Gen-I Photopyrometer	24
6. Front-Lighted Laser Photograph of Track G Model	25
7. Isothermal Contour Map of Nosetip—Gen-I Photopyrometer	26
8. Temperature Scans Across Nosetip—Gen-I Photopyrometer	27
9. Self-Luminosity Photograph of Track G Model—Gen-II Photopyrometer	28
10. Photograph of Recovered Track G Model	29
11. Isothermal Contour Map of Nosetip—Gen-I Photopyrometer	30
12. Temperature Scans Across Nosetip—Gen-II Photopyrometer	31
13. Self-Luminosity Photograph of Track G Model—Gen-I Photopyrometer	32
14. Photopyrometer System Temperature Measurement Uncertainty	33

<u>Figure</u>	<u>Page</u>
15. Flare Exposure Test Setup	34
16. Temperature Scans—Flare Effects Test Results	35
17. Predicted and Measured Graphite-Arc Lamp Temperature Profiles	41

TABLES

1. High-Speed Image Intensifier/High-Speed Photopyrometer State-of-the-Art History	42
2. Measurement Ranges for Track G Photopyrometers	43
3. Photographic Characteristics of Track G Photopyrometers	44

APPENDIXES

A. Image Intensifiers	45
B. Image Spreading Effects	48

1.0 INTRODUCTION

The aeroballistic range is an excellent ground test facility for simulating reentry into the earth's atmosphere (Refs. 1 through 3). Much aeroballistic range testing is concerned with reentry nosetip materials evaluations. The velocity/pressure conditions can be duplicated, and atmospheric particulate fields (rain, snow, ice, dust) can be generated.

A parameter of primary importance during materials evaluations is the in-flight temperature of the nosetip material being tested. Such temperature data are obtained by photopyrometry measurements at discrete locations along the flight paths. A photographic pyrometry technique has been employed successfully for a number of years in the 1,000-ft Hyperballistic Range (G)* of the von Kármán Gas Dynamics Facility (VKF) for obtaining these critical measurements (Refs. 3 through 12).

The key component used in the ballistic range photopyrometry technique is an image intensifier. The overall sensitivity of the photopyrometer is determined primarily by the spectral response and gain of the image intensifier; detection of longer wavelength radiation and/or greater intensification (higher gain) allows measurements of lower temperatures.

The initial aeroballistic range photopyrometry systems (Refs. 3, 5, 7, 8, 11, and 12) were developed around 1970 for use during ablation and erosion testing wherein surface temperatures of interest generally fell within the 3,000- to 4,000-K range. These systems employed then state-of-the-art, proximity-focused (diode type) image intensifiers with S-11 spectral response (0.35 to 0.65 μm) and with relay lenses for transferring the intensified image to the recording film. The lower temperature measurement limit was about 2,800 K.

Subsequently, other types of aeroballistic range, reentry materials testing required measurements of surface temperatures at levels below the 2,800-K limit of the initial systems. It thus became a goal of instrumentation research efforts to extend the lower measurement limits for Range G photopyrometers. Close liaison has been maintained with commercial manufacturers to ensure prompt evaluation of the latest image intensifier technology for photopyrometer applications. It is fortunate that manufacturers have since developed several significantly advanced types of image tubes. As these new state-of-the-art devices became available, work was directed toward design, fabrication,

*Henceforth in this report, Range G and Track G are the names used, respectively, for the 1,000-ft Hyperballistic Range (G) when operated in the free-flight and track-guided modes of operation.

and evaluation of new "low temperature" photopyrometers. Table I summarizes chronologically the state-of-the-art intensifiers and the corresponding resulting extensions of the lower temperature measurement capability.

Some of the more recently developed photopyrometers—those types currently applied to surface temperature measurements—are described herein. The utility of these systems is illustrated through presentations of nosetip surface temperature data acquired during recent reentry materials evaluation tests.

2.0 TRACK G SYSTEMS

All photopyrometers presently used in Track G employ image intensifiers developed in either 1975 (Gen-I) or 1976 (Gen-II) (Table 1). These types of image intensifiers are described in Appendix A. The advanced photopyrometers were used initially for measurements during free-flight tests in Range G. Track G (Ref. 2), designed specifically to facilitate materials evaluation testing, became operational in early 1977.* Since that time, all materials evaluation testing has been conducted in this facility. The photopyrometer systems described here are the track-compatible versions.

2.1 SYSTEM DESCRIPTION

A Track G photopyrometer system is shown schematically in Fig. 1. The image intensifier camera is attached to the track mechanism inside the range tank, much closer to the test model than was the case with Range G (free-flight) systems where large viewfields were necessary to accommodate flight-path dispersions. This ability to move closer to the model results in better photographic resolution and allows use of smaller-diameter intensifier tubes. Overall magnification with the arrangement of Fig. 1 is 0.3, and object-plane resolvability** is approximately 0.006 in. (Corresponding values for Range G systems were 0.15 and 0.012 in. for uprange systems and 0.08 and 0.024 in. for downrange systems.)

*In the track mode of operation for the ballistic range, the gun-launched test article is confined to a straight-line trajectory by four surrounding guide rails. The facility is designed so that models can be launched at velocities up to 20,000 ft/sec, guided through 1,000 ft of controlled test environment, and recovered without damage in a 500-ft-long decelerator tube. This unique facility overcomes aeroballistic range limitations associated with dispersion of the free-flight model and the inability to recover models intact.

**"Object-plane resolvability" refers to the minimum distance between two points on the object that allows these points to be resolved unambiguously in the image.

As shown in Fig. 1, a front-surface mirror placed just inside the track tube affords a viewing angle of 5 deg from head-on. This viewing angle, desirable for near-normal viewing of the stagnation point regions of nosetips being tested, tends to minimize motion blur. For example, an exposure time of 100 nsec results in motion blur of only 0.0016 in. for a model velocity of 15,000 ft/sec.

The design of power supply electronics allows selection of any one of several exposure durations (in effect, dynamic measurement ranges) for the pyrometer. The normally used exposure durations and corresponding dynamic measurement ranges for all current Track G photopyrometry systems are presented in Table 2. The dynamic ranges given in Table 2 are those achieved when the camera lens (Fig. 1) is operated at $f/11$. This is the lowest f /number (largest aperture diameter) that will satisfy depth-of-field requirements for track application. Pertinent photographic characteristics of the Track G photopyrometers are summarized in Table 3.

Track G photopyrometer systems are mechanically designed so that the image intensifier cameras can be removed conveniently and transported to the laboratory for calibration. Mounting is such that good registration is achieved when the cameras are reinstalled on the track mechanism; only minor adjustments are required for realignment. The five available photopyrometer systems listed in Table 2 can be operated at any five of six possible locations along the 1,000-ft test section of Track G. Two of the Gen-I systems listed in Table 2 employ special low-flare image intensifiers. These intensifiers, which became available for purchase in 1977, incorporate internal antireflective coatings that drastically reduce image spreading effects (Appendix B). Manufacturers are presently investigating techniques that might offer similar improvements to Gen-II intensifiers; however, the antireflective coating technique (Appendix B) used in the low-flare, Gen-I devices cannot be applied to the more complex Gen-II systems.

2.2 CALIBRATION

Blackbody sources are maintained as temperature standards in the laboratory. A graphite-arc lamp and filter set are used to provide discrete reference temperatures of, nominally, 3,800, 3,200, 2,900, 2,700, 2,200, and 1,700 K. A conventional (cavity-type) blackbody radiator is used to produce calibration temperatures in the 1,000- to 1,900-K range. Both calibration sources are traceable to the National Bureau of Standards; temperatures produced by these sources are known to within ± 15 K.

Before data are recorded, a photopyrometer is set up in the laboratory to view the appropriate calibration source. (Calibration sources used for the various systems and dynamic ranges are listed in Table 2.) Care is taken to match the optical path with that to be used for measurements in Track G. The calibration path includes a front-surface mirror and has physical dimensions identical to those in Fig. 1.

Once calibration curves are established, the density information from the nosetip images may be converted to temperature information. The remaining data reduction procedures concern manipulation of this temperature information into desired presentation formats. The calibration curve data along with model image density data are entered into a computer to generate an isothermal contour map of the nosetip surface and single-scan temperature profiles of the model nosetip for each Track G photopyrometer station.

4.0 TYPICAL RESULTS

A self-luminosity photograph of a model nosetip as recorded with a Gen-I photopyrometer in Track G is shown in Fig. 5. Related calibration data are shown in Figs. 2a and 4a. A broadside, front-lighted laser photograph (Refs. 3, 4, 9, and 10) recorded during this same shot is shown in Fig. 6. Temperature data extracted from the photograph of Fig. 5 are illustrated by Figs. 7 and 8. Figure 7 is an isothermal contour map, and Fig. 8 shows horizontal and vertical single-scan temperature profiles. The locations of these scans relative to the isothermal contour map are as indicated in Fig. 7.

A self-luminosity photograph obtained with a Gen-II photopyrometer in Track G is shown in Fig. 9. Applicable calibration data are shown in Figs. 2b and 4b. Figure 10 is a photograph of the recovered test model. Reduced temperature data are shown in Figs. 11 and 12; Fig. 11 is the isothermal contour map, and Fig. 12 shows the single-scan temperature plots. Obviously, these important temperature data could not have been acquired using pre-1976 photopyrometers (Table 1).

The enlarged self-luminosity photograph in Fig. 13 is an example of the use of a Gen-I, low-flare, image intensifier in Track G and dramatically illustrates the photographic quality obtainable with such a system. The clarity permits examination of the hemispherical nosetip in the detail usually associated with static, front-lighted photographs.

5.0 CONDITIONS AND ASSUMPTIONS

Temperatures measured with photopyrometers are, by the nature of the measurement technique, brightness temperatures. The measured temperatures are equivalent to true temperatures only if the surfaces being measured radiate in a strictly incandescent manner (according to the familiar Planck equation) and if the emissivity of the surfaces is unity. Contributions of radiation from any extraneous sources must be negligible.

Most of the reentry nosetip materials evaluated in the aeroballistic range are made of carbon or compounds thereof. It is known that these materials are incandescent radiators and, further, that the emissivities for the materials are close to unity throughout the spectral range of Track G photopyrometers (i.e., these materials closely approximate blackbody radiators). It is only for these carbon materials that measurements of true temperature are inferred; the data reduction scheme tacitly assumes that emissivity is unity.

To ensure that the photopyrometry systems detect only incandescent radiation from the nosetip surface and thus provide realistic measurements of temperature, it is necessary to quench or considerably diminish chemiluminescence and shock cap radiation. This is achieved in Track G by use of helium-filled chambers at each photopyrometry station. Each photograph (surface temperature measurement) is recorded while the model is temporarily in "flight" within an inert helium atmosphere.

6.0 MEASUREMENT UNCERTAINTY

Uncertainty in model surface temperature measurements is attributable to sources of error that can be classified in two major categories—pyrometer system-related sources and test-related sources. The several possible error-producing factors in both major categories are discussed, and empirical data are presented describing the effects of some of these factors on uncertainty.

6.1 SYSTEM-RELATED ERROR SOURCES

If the intrinsic features of the photopyrometry technique are considered, several possible sources of error associated directly and solely with the measurement system may be listed:

1. calibration source uncertainty
2. exposure time variation*
3. intensifier gain variation*
4. film-to-film inconsistency
5. film processing variation
6. optical system differences*
7. calibration curve interpolation
8. photocathode spatial nonuniformity
9. microdensitometer imprecision

As mentioned previously, the graphite-arc lamp and blackbody source used to produce calibration temperatures are traceable to the National Bureau of Standards and are known to within ± 15 K.

* Between calibration and data recording.

A number of the possible error sources listed above (2 through 6) were thoroughly investigated during development of the photopyrometry technique, and temperature uncertainty contributions from these sources were found to be minimal (Refs. 11 and 12). Experiments revealed no measurable variation in exposure time or gain from photograph to photograph with Track G photopyrometer systems. Variations in sensitivity from film to film within a particular batch of film were negligible.

Errors that can arise from variations in development time, developer potency, developer temperature, etc. are avoided through simultaneous processing of both data negatives and calibration negatives. Extreme care is taken to match the optical paths during calibration and data recording so that errors from this additional source are minimal.

Photopyrometer calibration curves (e.g., Fig. 4) are normally constructed by connecting discrete temperature calibration points with straight-line segments. This approach "curve fits" the calibration data very well; for calibration curves such as those shown in Fig. 4, errors arising from straight-line interpolation (as opposed to a polynomial curve fit) between calibration points are less than 20 K. The trend toward nonlinearity near the high temperature/density end of the calibration curves is a result of approaching system saturation. The sensitivity of each photopyrometer is adjusted in such a manner as to minimize this saturation effect and the resulting curvature in the calibration curve.

The remaining possible error sources (8 and 9 above) are the primary contributors to photopyrometer system measurement uncertainty (for measurements of an ideal source). Manufacturers' specifications indicate that response across the photocathode surface of an image intensifier of the type used in Track G photopyrometers may vary by as much as 10 percent; i.e., certain points on the phosphor surface (see Appendix A) may differ in intensity by 10 percent from average value when the photocathode surface is uniformly illuminated. The digital scanning microdensitometer used to extract information from data and calibration negatives has a precision error of $\pm 0.01D$ in reading photographic film density.

Two of the error sources listed above, calibration source uncertainty (1) and calibration curve interpolation (7), contribute bias errors to photopyrometer measurements. The bias errors have estimated magnitude but unknown direction, ± 15 K and ± 20 K, respectively. The remaining sources contribute solely to random error.

The effects of these contributions to uncertainty were quantified by analyzing results of laboratory experiments consisting of repeated static measurements of the available temperature sources—a graphite-arc lamp and cavity-type blackbody. The

experimental approach taken has adequately assessed the uncertainty contributions from all the possible sources of system error listed previously.

Data for uncertainty analyses were acquired by using Gen-I and Gen-II photopyrometers, calibrated in the manner described in Section 2.2, to make measurements of the graphite arc and blackbody sources at several known temperatures within both ranges (Table 2) of each photopyrometer. A set of 5 to 9 measurements was made for each temperature; the source was imaged onto a different area of the intensifier photocathode for each measurement in each set.

A widely used standard format for statement of uncertainty is given in Ref. 13:

$$U = \pm (B + t_{95}S) \quad (1)$$

where U is the total measurement uncertainty, B is the bias limit, S is the precision index, and t_{95} is the 95th percentile point for the two-tailed Students "t" distribution.

For the photopyrometer case, as mentioned above, there are two contributors to bias uncertainty of estimated magnitude and unknown direction. The bias term (B) in Eq. (1) is the root-sum-square (Ref. 13) of these two components.

$$B = \pm \sqrt{15^2 + 20^2}$$

or $B = \pm 25^\circ\text{K}$

The precision index (S), also called the best estimate of the standard deviation, is given by

$$S = \sqrt{\frac{\sum_{i=1}^N (T_i - \bar{T})^2}{N - 1}} \quad (2)$$

where N is the number of measurements made, and \bar{T} is the average value of individual measurements T_i .

The statistic t_{95} [Eq. (1)] is a function of N . A tabulation of this common statistic is given in Ref. 13. For example, $t_{95} = 2.571$ for $N = 5$; and $t_{95} = 2.262$ for $N = 9$.

Precision index values [Eq. (2)] were calculated for each set of experimental temperature measurements, then multiplied by the appropriate t_{95} values to give the random uncertainty for each case. Total system uncertainty values, U , [Eq. (1)] are plotted as a function of temperature in Fig. 14.

It can be seen from Fig. 14 that uncertainty increases toward the high-temperature end of each dynamic range for each photopyrometer. This is a consequence of the approximately linear relationship of the reciprocal of temperature with film density illustrated in the calibration curves of Fig. 4. It is evident that for a given uncertainty in film density, the corresponding uncertainty in temperature is considerably greater for the higher temperatures (densities). In addition, the typical trend away from linearity at the higher film densities (Fig. 4) is in such a direction as to further accentuate this high-temperature measurement uncertainty effect. Figure 14 does indicate, however, that it is possible to keep the total system uncertainty to within ± 130 K for measurements over the range of 1,250 to 4,000 K by judicious choices of photopyrometer type and dynamic range.

6.2 TEST-RELATED ERROR SOURCES

The experimental uncertainty assessment and the resultant data of Fig. 14 apply only to the photopyrometry systems and their calibrations. Figure 14 indicates the measurement uncertainty that can be expected when making temperature measurements of an ideal temperature source. In the aeroballistic range application, there are possible sources of error related to or caused by the source (test model) being measured:

1. motion blur
2. chemiluminescence
3. shock cap air radiation
4. heat shield luminosity
5. wake radiation
6. nosetip hot spots

Considerable effort has been expended toward eliminating or minimizing these possible sources of error.

The near head-on viewing angle (Fig. 1) of photopyrometers tends to minimize motion blur. The slight motion of the model image during photographic recording should have little effect on temperature measurements. In fact, the blur is, in many cases, less than the optical resolution capability of the photographic systems (see Table 3).

A technique has been devised and implemented for reduction of the effects of the above possible error sources chemiluminescence (2) and shock cap air radiation (3) to insignificant levels. As mentioned previously, each photopyrometer photograph (surface

temperature measurement) is recorded while the test model is temporarily in flight within an inert helium atmosphere. Chemical reactions (e.g., oxidation) and the resulting chemiluminescence are quenched when the test model enters the inert gas. The shock cap brightness temperature while the test model is in flight (at typical reentry conditions) in the helium environment is estimated to be 1,000 K or less. (This compares with a value near 2,400 K for flight in air) Thus, radiation from a helium shock cap falls below the measurement threshold of even the high-sensitivity, Gen-II photopyrometers.

Heat shield luminosity and wake radiation (4 and 5 above) are also possible sources of measurement error because they can introduce extraneous radiation into the resultant photopyrometer image of the nosetip. If these sometimes extremely intense radiation sources appear in the viewfield, image spreading effects (Appendix B) may result: Portions of the images of the heat shield and/or wake may be spread onto portions of the image of the nosetip. In such cases, temperature measurements of the affected portions of the nosetip can be artificially elevated. Control measures are taken to minimize these problems in Track G. Heat shield materials that produce low levels of luminosity are used, and optical restrictors are employed to limit the photopyrometer field-of-view by excluding most of the radiant wake from view.

The most troublesome test-related source of error is that caused by hot spots on the nosetip (6 above) of the model under measurement. In making desired measurements of a "low" temperature surface that is close to a significantly higher temperature region on the nosetip, image spreading effects (Appendix B) can become restrictive. These effects are manifested in image flare or halo. Measurements of temperature distributions similar to the type depicted in Fig. 9 (a "cool" stagnation point region surrounded by a higher temperature ring) are subject to errors caused by such effects. Figure 12 indicates that there is little, if any, error in this particular case (Figs. 9, 11, and 12) since measured temperatures in the stagnation point region are very near the background level (the 1,250-K lower measurement limit). However, distributions of this type with "ring" temperatures a few hundred degrees higher than those indicated by Fig. 12 might be expected to elevate artificially measurements of "cool" temperatures in the stagnation point region.

Image spreading, or flare, effects (described in Appendix B) have been examined experimentally for the photopyrometers used in Track G. The magnitude of the measurement error depends on the temperature differences, relative areas, and separations of the "hot" and "cool" surface zones, and on the particular image tube in use. Because of the complexity of the problem, it has not been possible to produce all-inclusive empirical data defining image flare limitations. However, laboratory experiments using the arrangement shown in Fig. 15 were conducted in efforts to quantify flare effects, and the experimental results (Fig. 16) have proved useful in shot-by-shot assessments of data

quality. These data in Fig. 16 typify the flare characteristics of the three types of systems presently in use in Track G: Gen-II, Gen-I (standard), and Gen-I (low-flare). Data are shown for both the low- and high-temperature ranges of these systems.

A standard calibration source (blackbody cavity or graphite-arc lamp with appropriate temperature adjustment filters) was used as the target for the photopyrometer systems in the laboratory experiments. Test exposures were obtained at each temperature of interest for the three systems evaluated. The calibration source provided a high-temperature spot adjacent to a low-temperature background surface. The artificial elevation of the apparent temperature of this adjacent region thus provided an indication of the flare-introduced measurement uncertainty.

Each of the laboratory results in Fig. 16 shows an overlay of temperature scan data obtained at several calibration source temperatures for the photopyrometer system indicated. These data are laboratory results that are analogous to the test results depicted in the plots of Figs. 8 and 12. The scans in Fig. 16a are for the Gen-II system operated at the low-temperature dynamic range (1,000- or 300-nsec exposure times). The target in this case was a blackbody cavity with a 0.2-in.-diam exit circle. Each minor division along the distance scale in Fig. 16a represents one microdensitometer aperture or 0.013 in. in the source (object) plane. As can be seen in Fig. 16a, this finite microdensitometer scanning aperture leads to some edge effects, but these are generally confined to within ± 1 division/aperture of the indicated source edges. The data in Fig. 16a indicate that no significant flare exposure occurs for hot spot temperatures as high as 1,600 K. However, a slight flare zone does exist and extends approximately 0.25 in. from the source edge for a hot spot temperature of 1,800 K.

Figure 16b shows temperature scans for the Gen-II system operated at the high-temperature dynamic range (100- or 30-nsec exposure times). The target in this case and in all Gen-I system evaluations (Figs. 16c through f) was the graphite-arc lamp. The width of the arc source is not as well known as that of the blackbody cavity because the actual size of the source varies slightly during normal arc operation. The temperature distribution is not uniform across the arc source (positive electrode) as can be seen from the example shown in Fig. 17; predicted (Ref. 14) and measured (including flare and edge effects) temperature profiles of the graphite-arc source, for a particular case, are shown for comparison. Photopyrometer calibrations (Section 2.2) are made using a 0.08-in.-diam spot at the center of the source; temperatures are predicted (Ref. 14) to be uniform within this spot. The effective arc source width has been determined to be 0.18 in. The temperature scans for 1,750 K and 2,000 K in Fig. 16b follow the arc source contour without significant flare. Some flare-induced elevation of the background does occur for the arc source temperature of 2,200 K, and considerable flare elevation—extending 0.28 in. from the source—occurs for the arc source temperature of 2,550 K.

Temperature scans for the standard and low-flare Gen-I systems are shown in Figs. 16c through f. The considerable improvement offered by the low-flare system is evident in these figures. Comparison of Figs. 16c and e shows that a temperature of 3,200 K is required in the low-flare system to produce the same flare effect as those associated with a 2,700-K temperature in the standard Gen-I system. The superior characteristics of the low-flare system are further pointed out by Figs. 16d and f, showing the high-temperature dynamic range responses.

6.3 SUMMARY OF TEMPERATURE MEASUREMENT UNCERTAINTY

The primary system-related error sources are photocathode spatial nonuniformity and microdensitometer imprecision. Laboratory experiments were used to characterize the overall effects of solely system-related error sources on measurement uncertainty. The results of this system uncertainty determination are shown in Fig. 14. Optimum data accuracy can be achieved through judicious choices of photopyrometer type and dynamic range to fit the expected range of nosetip temperatures. The data of Fig. 14 indicate that, if proper choices of photopyrometer/range are made, any temperature within the 1,250- to 4,000-K range can be measured with a system-related uncertainty of less than 130 K.

The main test-related sources of measurement error are heat shield luminosity, wake radiation, and excessively hot surfaces on the model nosetip. Control measures have proved successful in greatly reducing heat shield and wake radiation problems, and an experimental examination of the problem resulting from the presence of hot spots on the nosetip has been conducted in the laboratory. Measurement uncertainty attributable to flare effects caused by these hot spots must be assessed on an individual shot basis. Problem areas can usually be identified by study of photopyrometer photographs and reduced temperature data. In photographs dominated by flare effects, it is not possible to extract certain low temperature data with reasonable accuracy; therefore, it is very important that flare effects be kept at a minimum.

The control measures were effective for the Track G examples discussed here (Figs. 5 and 9), and no excessive hot spots were found on the nosetip; consequently, the resultant data plots (Figs. 7, 8, 11, and 12) are void of significant test-related uncertainties. The net uncertainties associated with these temperature data, then, are solely system related and are characterized by Fig. 14.

7.0 CONCLUDING REMARKS

Advanced photographic pyrometry systems have been developed in the AEDC-VKF and have demonstrated an expanded capability for measurements of surface temperature

distributions on the nosetips of models in flight in Track G. The latest (Gen-II) of these state-of-the-art photopyrometers allows surface temperature measurements as low as 1,250 K. A number of materials evaluation tests, characterized by a predominance of surface temperature levels below the measurement limits of previously used photopyrometers, are now performed successfully in Track G. A total temperature measurement range of 1,250 to 4,000 K can be covered in Track G through use of both Gen-I and Gen-II photopyrometers. Measurement uncertainty attributable solely to system-related sources can be kept within ± 130 K limits over this wide range of temperatures by proper selection of photopyrometer type and dynamic range. Measurement uncertainty attributable to flare must be assessed on an individual shot basis. Flare problem areas can usually be identified by study of the photopyrometer photographs and reduced temperature data. To achieve optimum temperature measurement accuracy, the photopyrometer type and exposure time (dynamic range) should be chosen to match the level and dynamic range of nosetip temperatures, and control measures should be employed to reduce extraneous radiation to insignificant levels.

REFERENCES

1. Callens, E. E., Jr. and Blanks, J. R. "Development of a Snow Erosion Test Capability for the Hyperballistic Range." Proceedings AIAA 13th Aerospace Sciences Meeting, MIT Press, Cambridge, Mass., n.d.
2. Norfleet, G. D., Hendrix, R. E., and Jackson, D. "Development of a Hypervelocity Track Facility at AEDC." Proceedings AIAA 15th Aerospace Sciences Meeting, Los Angeles, Calif., January 1977, paper 77-151.
3. Norfleet, G. D., Hendrix, R. E., Raper, R. M., and Callens, E. E., Jr. "Development of an Aeroballistic Range Capability for Testing Reentry Materials." Journal of Spacecraft and Rockets, Vol. 12, No. 5, May 1975, pp. 302-307.
4. Dugger, P. H. "Aeroballistic Range/Track Photographic Instrumentation Development." AEDC-TR-77-98 (ADA053591), April 1978.
5. Dugger, P. H. "Optical Instrumentation Studies in Aerospace Facilities—A Project Summary." AEDC-TR-72-141 (AD750866), October 1972.
6. Dugger, P. H. "Aeroballistic Range Instrumentation Development." AEDC-TR-76-146 (ADA030567), September 1976.

7. Hendrix, R. E. and Dugger, P. H. "Photographic Instrumentation in Hyperballistic Range (G) of the von Kármán Gas Dynamics Facility." Photographic Applications in Science, Technology and Medicine, Vol. 8, No. 5, September 1973, pp. 22-30.
8. Hendrix, R. E. and Dugger, P. H. "Instrumentation for an Aeroballistic Range Ablation Test Facility." 5th International Congress on Instrumentation in Aerospace Simulation Facilities, Record, Institute of Electrical and Electronics Engineers, Inc., New York, 1973, pp. 45-50.
9. Hendrix, R. E. and Dugger, P. H. "High-Speed Photography in the Aeroballistic Range and Track Facilities of the von Kármán Gas Dynamics Facility." Proceedings 12th International Congress on High-Speed Photography, Society of Photo-Optical Instrumentation Engineers, Bellingham, Washington, 1977.
10. Hendrix, R. E. and Dugger P. H. "Photographic Instrumentation in the VKF Aeroballistic Track Facilities." Proceedings 13th International Congress on High-Speed Photography, Tokyo, Japan, September 1978 (In publication).
11. Dugger, P. H., Bock, O. H., and Enis, C. P. "A High-Speed Photographic Pyrometer." Proceedings of the Technical Program, Electro-Optical Systems Design Conference-1971 East, Industrial and Scientific Conference Management, Inc., New York, 1971.
12. Dugger, P. H., et. al. "Photographic Pyrometry in an Aeroballistic Range." Proceedings SPIE 16th Annual Technical Meeting, San Francisco, Calif., October 1972.
13. Abernethy, R. B., Thompson, J. W. "Handbook--Uncertainty in Gas Turbine Measurements." AEDC-TR-73-5 (AD755356), February 1973.
14. Null, M. R. and Lozier, W. W. "The Carbon Arc as a Radiation Standard." Temperature: Its Measurement and Control in Science and Industry, ed. Charles M. Herzfeld, Vol. 3, Part 1, ed. F. G. Brickweede. Reinhold Publishing Corporation, New York, 1962, pp. 551-558.

Notes:

1. Magnification: 0.3
2. Distance along Optical Axis from Camera Lens to Focal Plane: ~36 in.

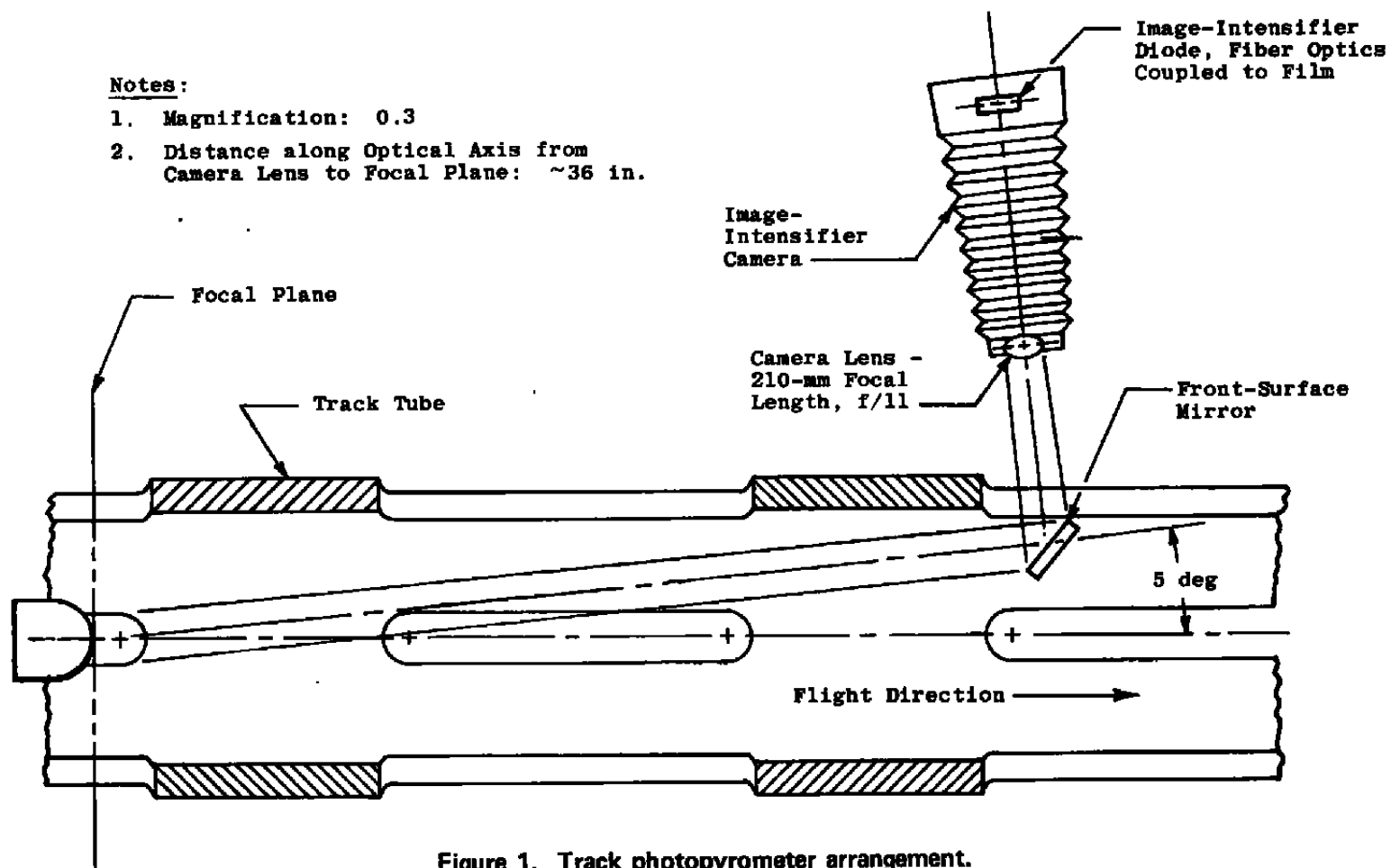
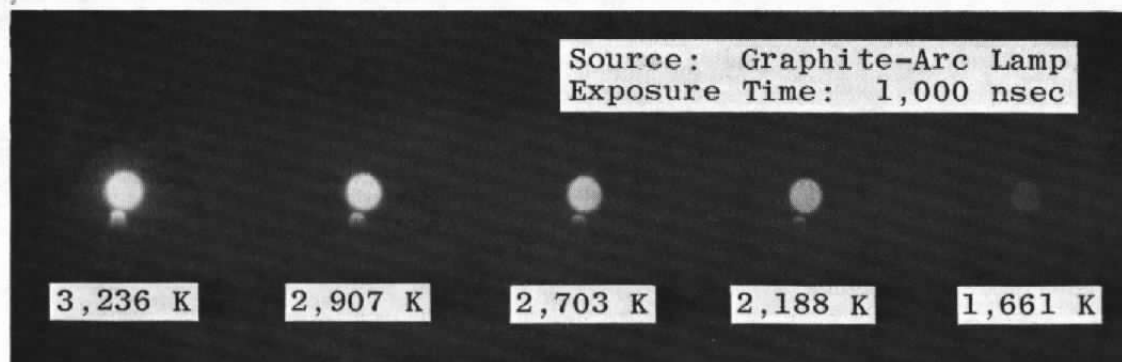
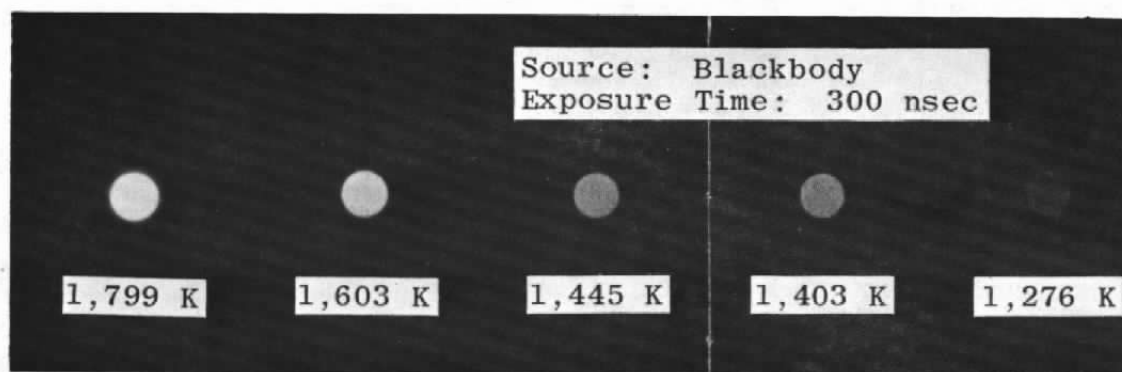


Figure 1. Track photopyrometer arrangement.



a. Gen-I photopyrometer



b. Gen-II photopyrometer

Figure 2. Typical photopyrometer calibration photographs.

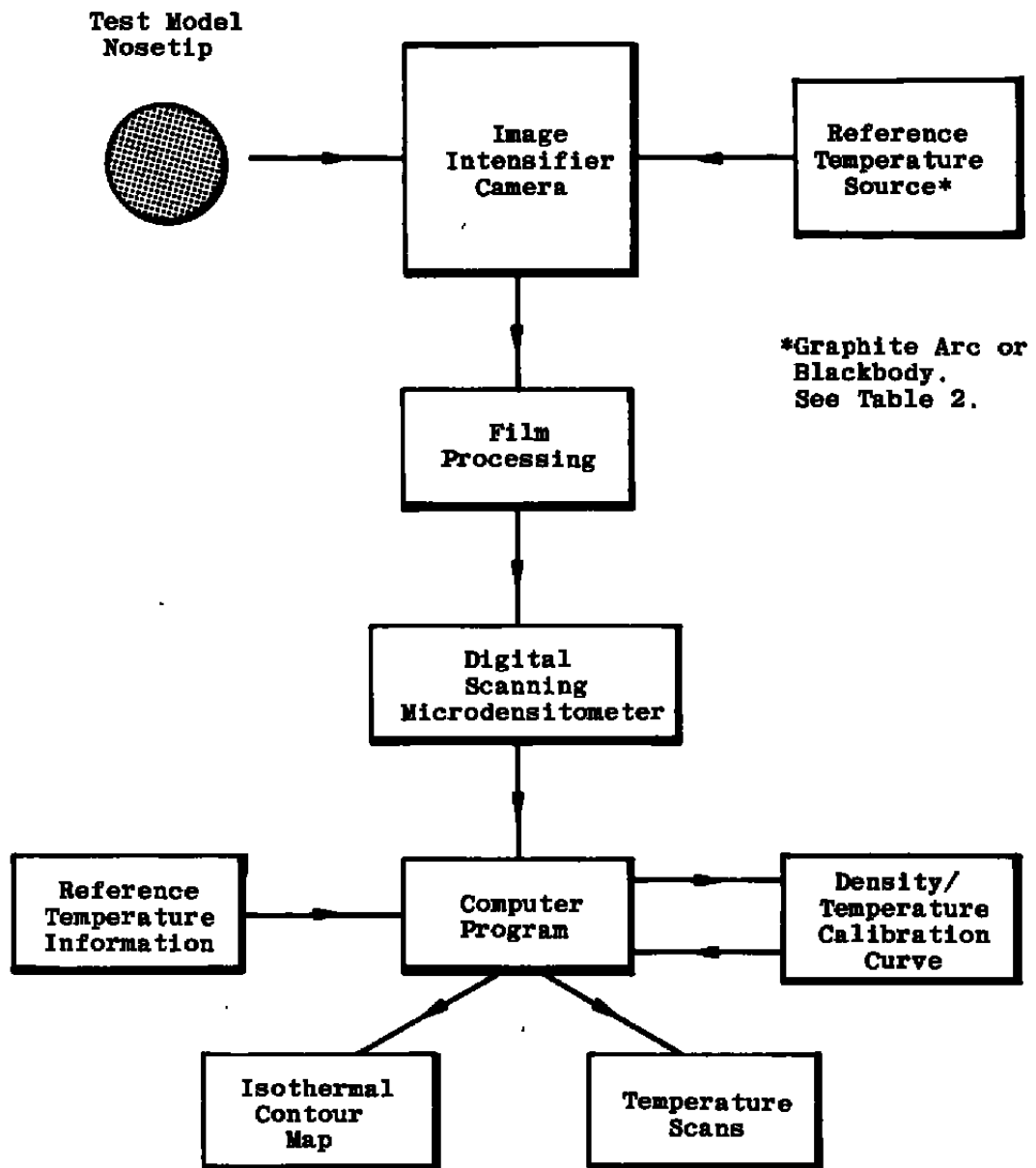
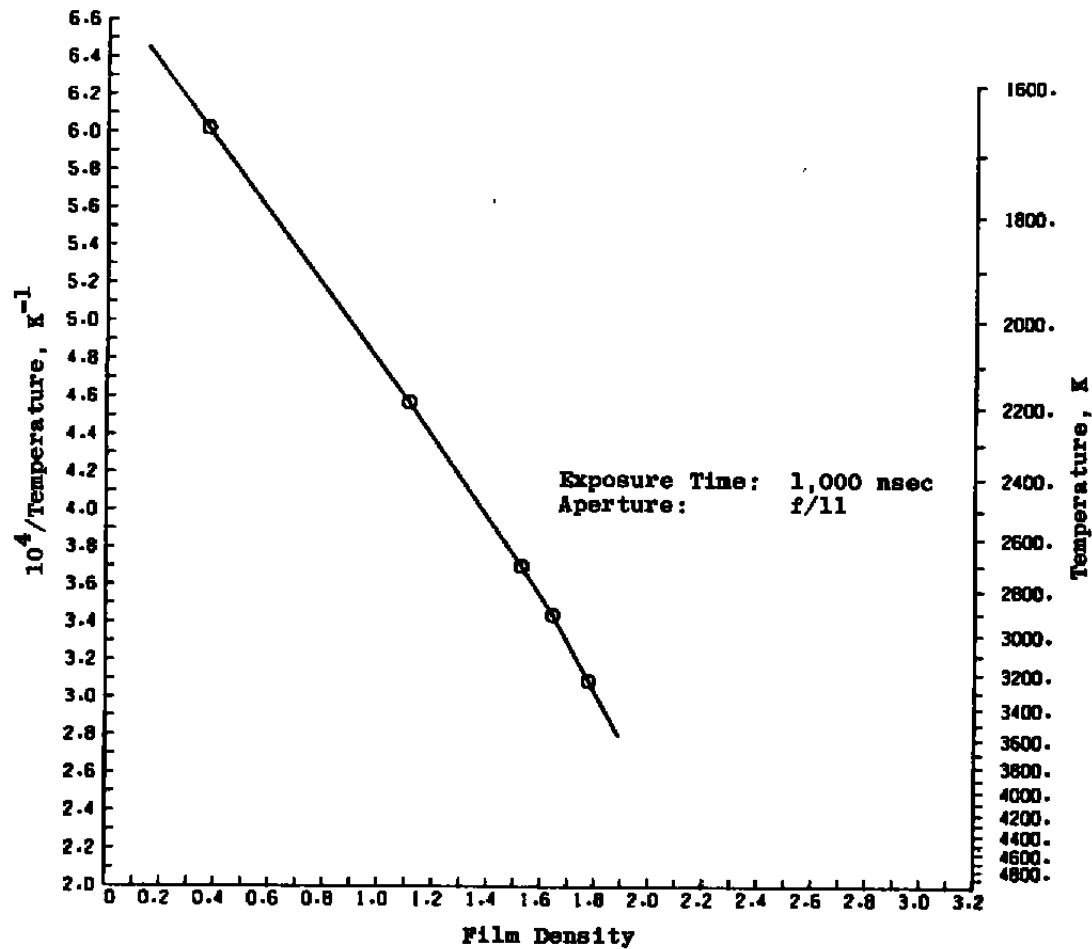
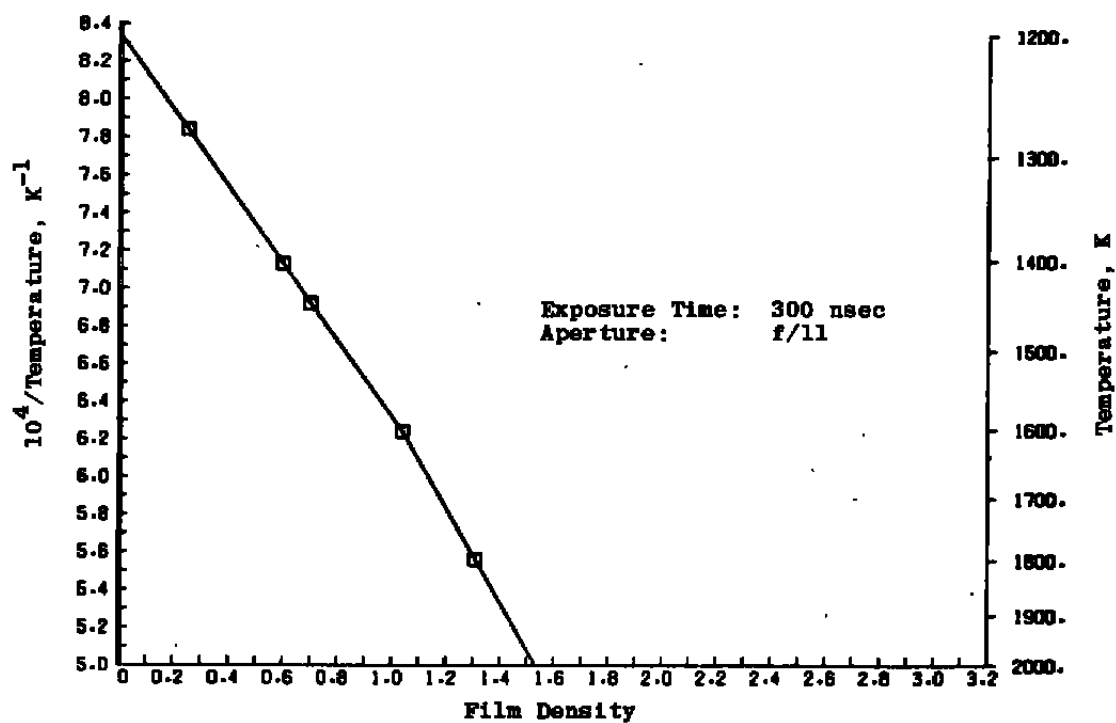


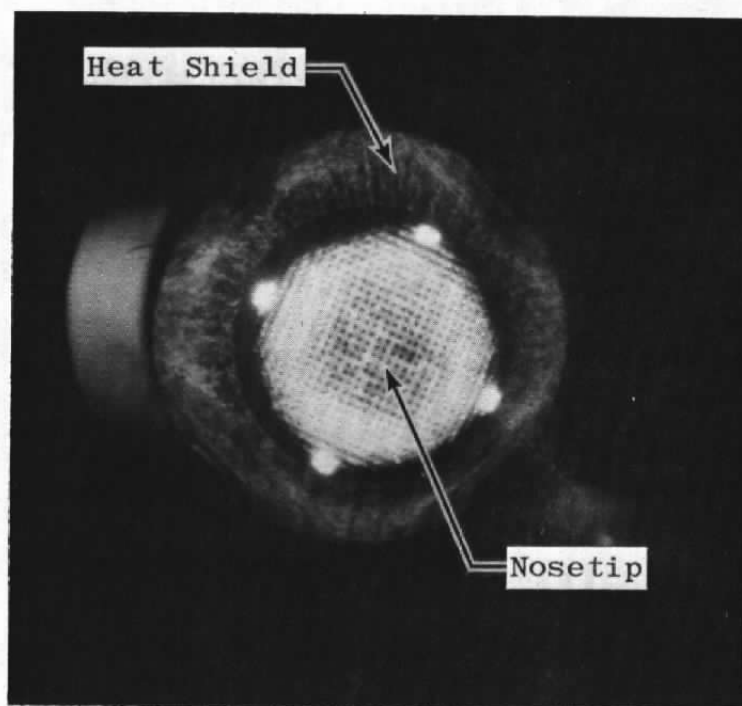
Figure 3. Data acquisition and reduction.



a. Gen-I photopyrometer
Figure 4. Photopyrometer calibration curves.



b. Gen-II photopyrometer
Figure 4. Concluded.



Model Velocity: 16,000 ft/sec
Nosetip Diameter: 1.6 in.
Viewing Angle: 5 deg from head-on
Exposure Time: 1,000 nsec

Figure 5. Self-luminosity photograph of Track G
Model-Gen-I photopyrometer.

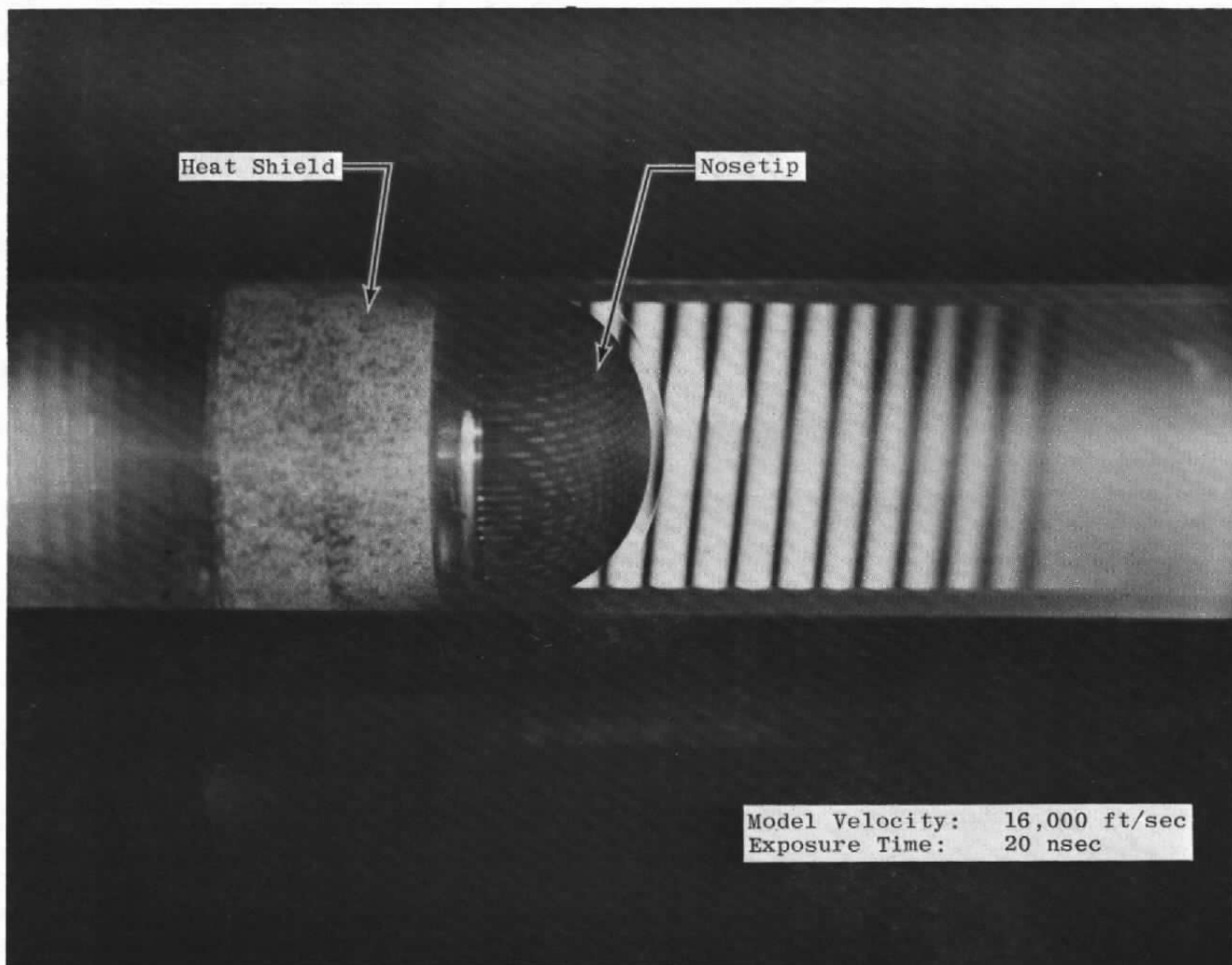
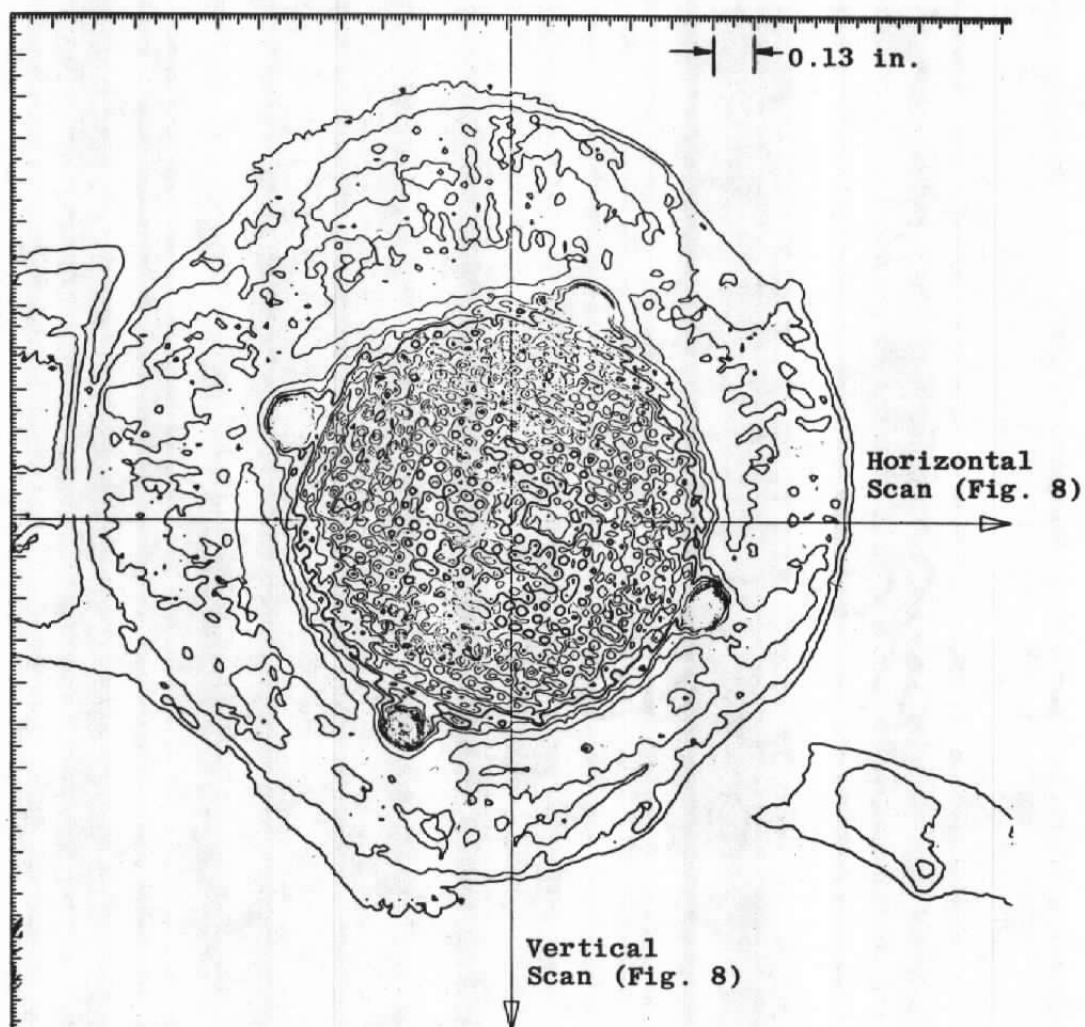


Figure 6. Front-lighted laser photograph of Track G Model.



<u>Legend</u>		Model Velocity:	16,000 ft/sec
Contour Intervals:	100 K	Nosetip Diameter:	1.6 in.
Heavier lines are 2,000-K isotherms.		Exposure Time:	1,000 nsec
		Viewing Angle:	5 deg from head-on

Figure 7. Isothermal contour map of Nosetip-Gen-I photopyrometer.

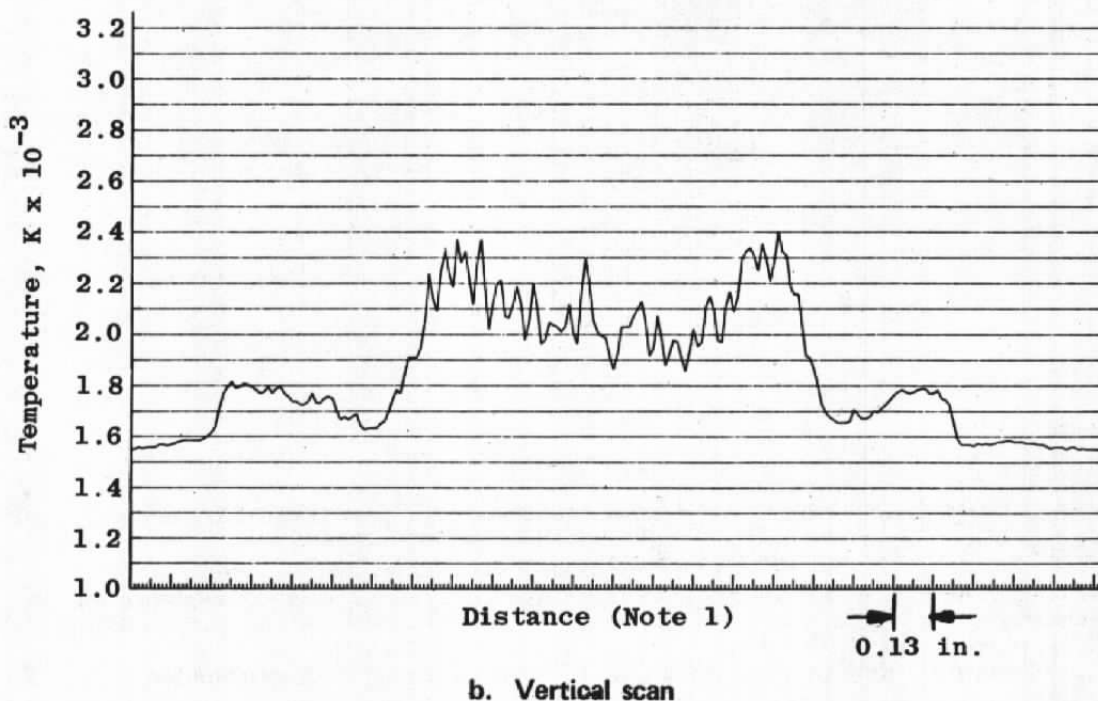
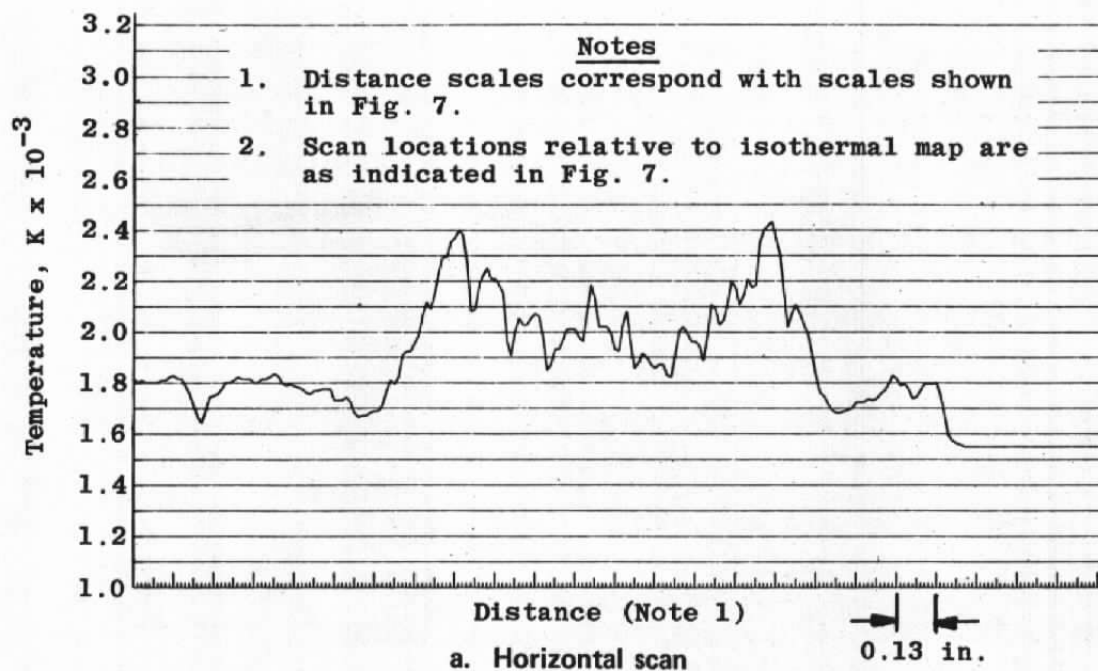
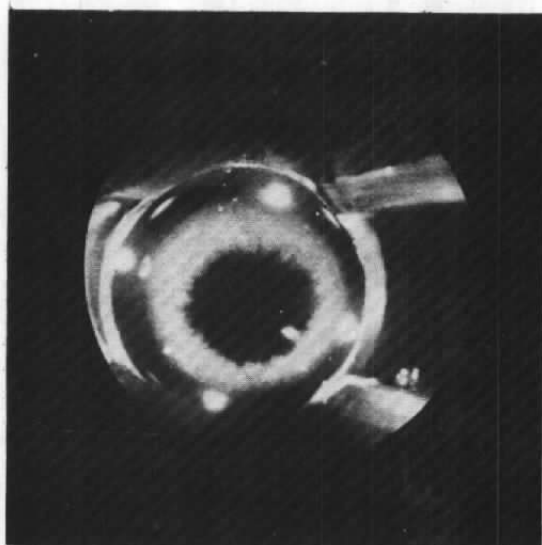


Figure 8. Temperature scans across nosetip—Gen-I photopyrometer.



Model Velocity: 16,000 ft/sec

Nosetip Diameter: 2.25 in.

Viewing Angle: 5 deg from Head-On

Exposure Time: 300 nsec

**Figure 9. Self-luminosity photograph of Track G
Model-Gen-II photopyrometer.**

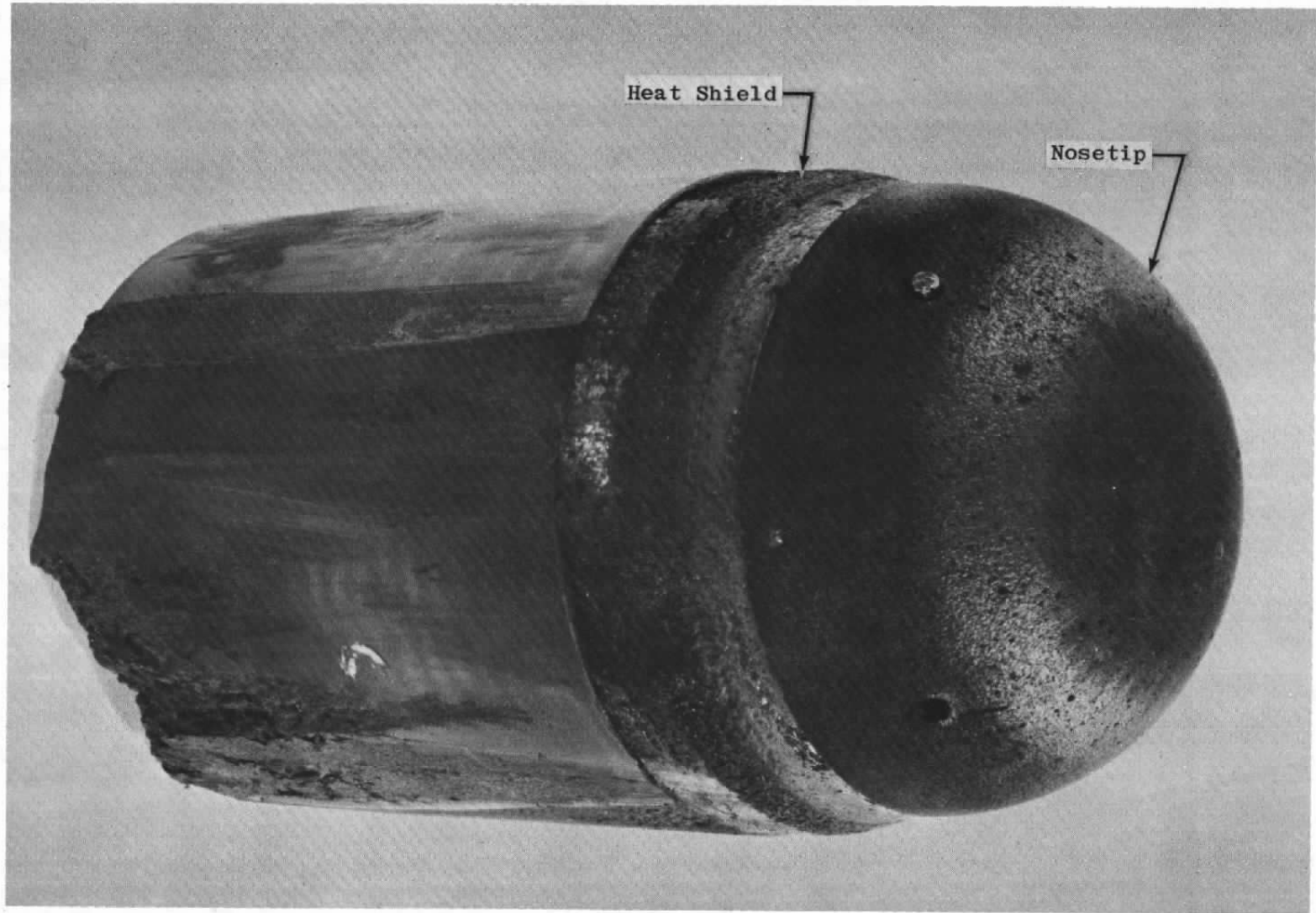


Figure 10. Photograph of recovered Track G Model.

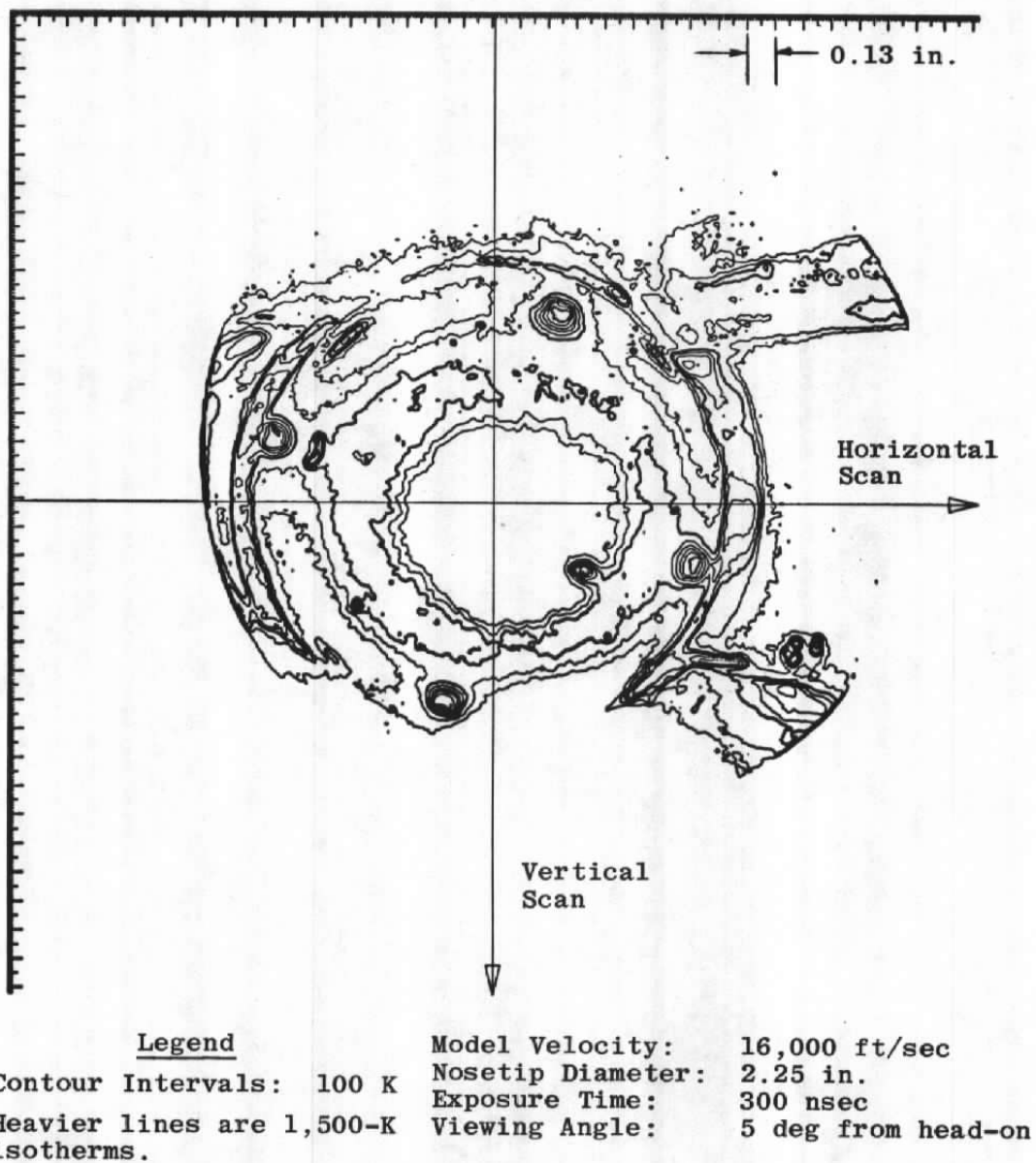
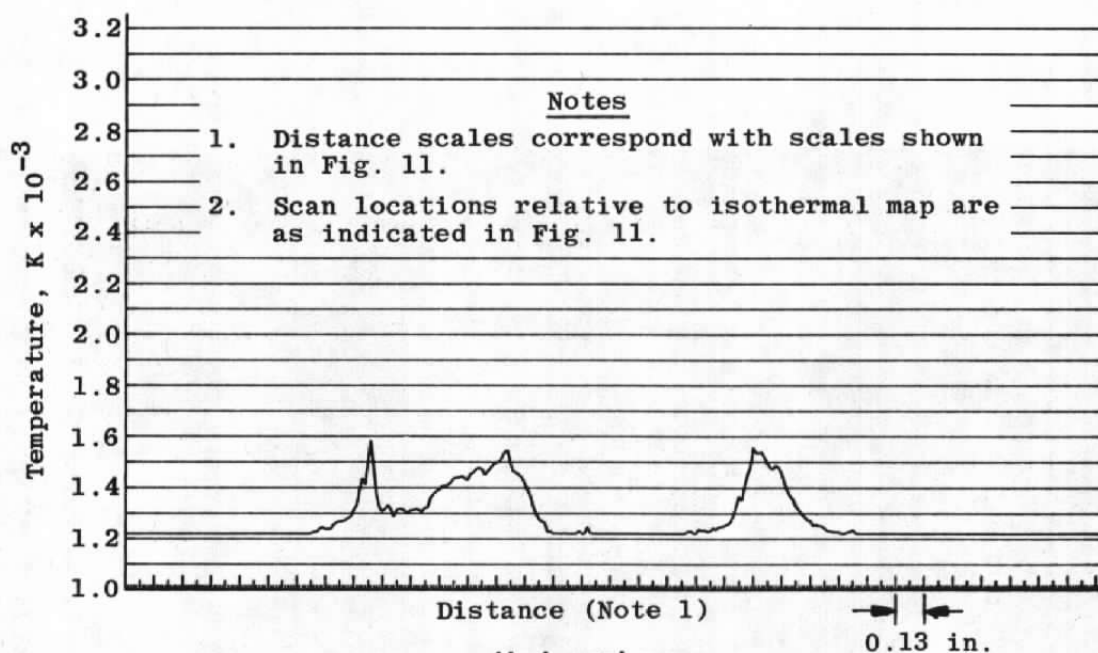
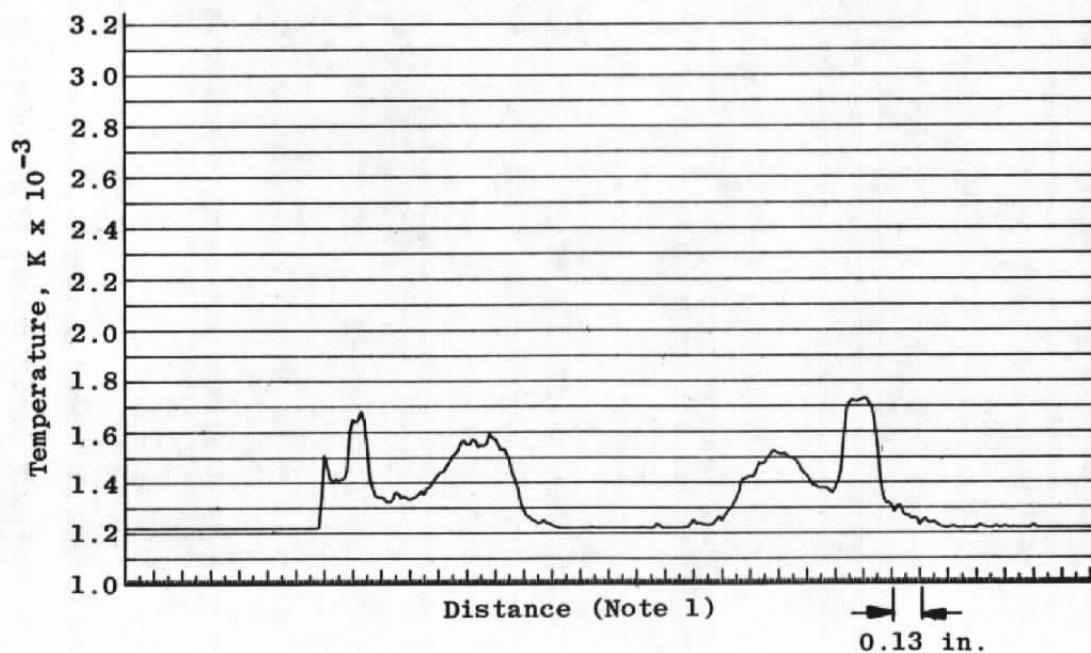


Figure 11. Isothermal contour map of nosetip-Gen-II photopyrometer.



a. Horizontal scan



b. Vertical scan

Figure 12. Temperature scans across nosetip—Gen-II photopyrometer.

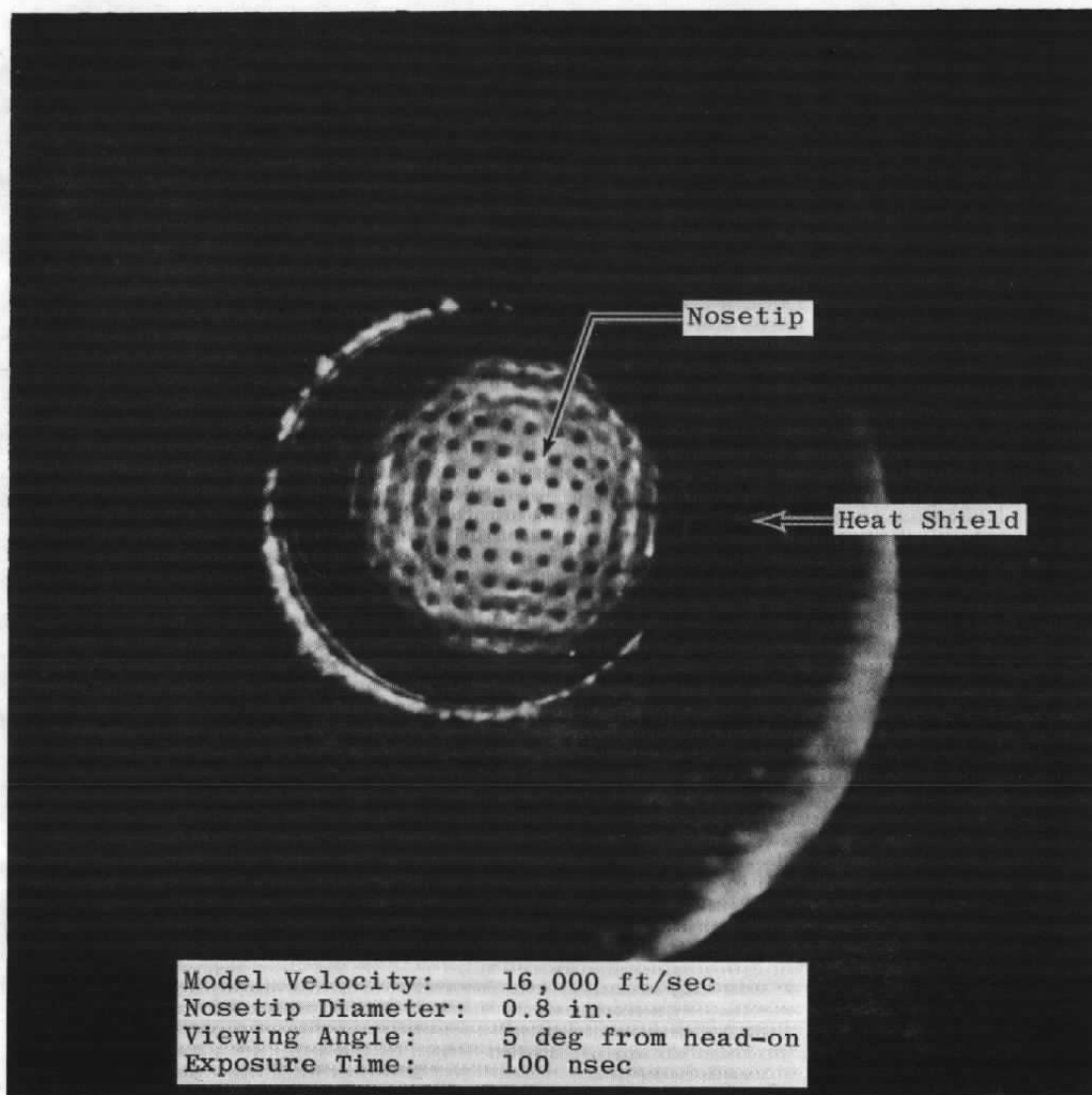


Figure 13. Self-luminosity photograph of Track G Model-Gen. I photopyrometer.

NOTES:

1. Each plotted point represents the result of a statistical analysis of multiple measurement samples at each particular temperature (see text).
2. The Gen-II system that operates at exposure times of 300 and 30 nsec has the same sensitivities, dynamic ranges, and, thus, uncertainties as the Gen-II system evaluated here.

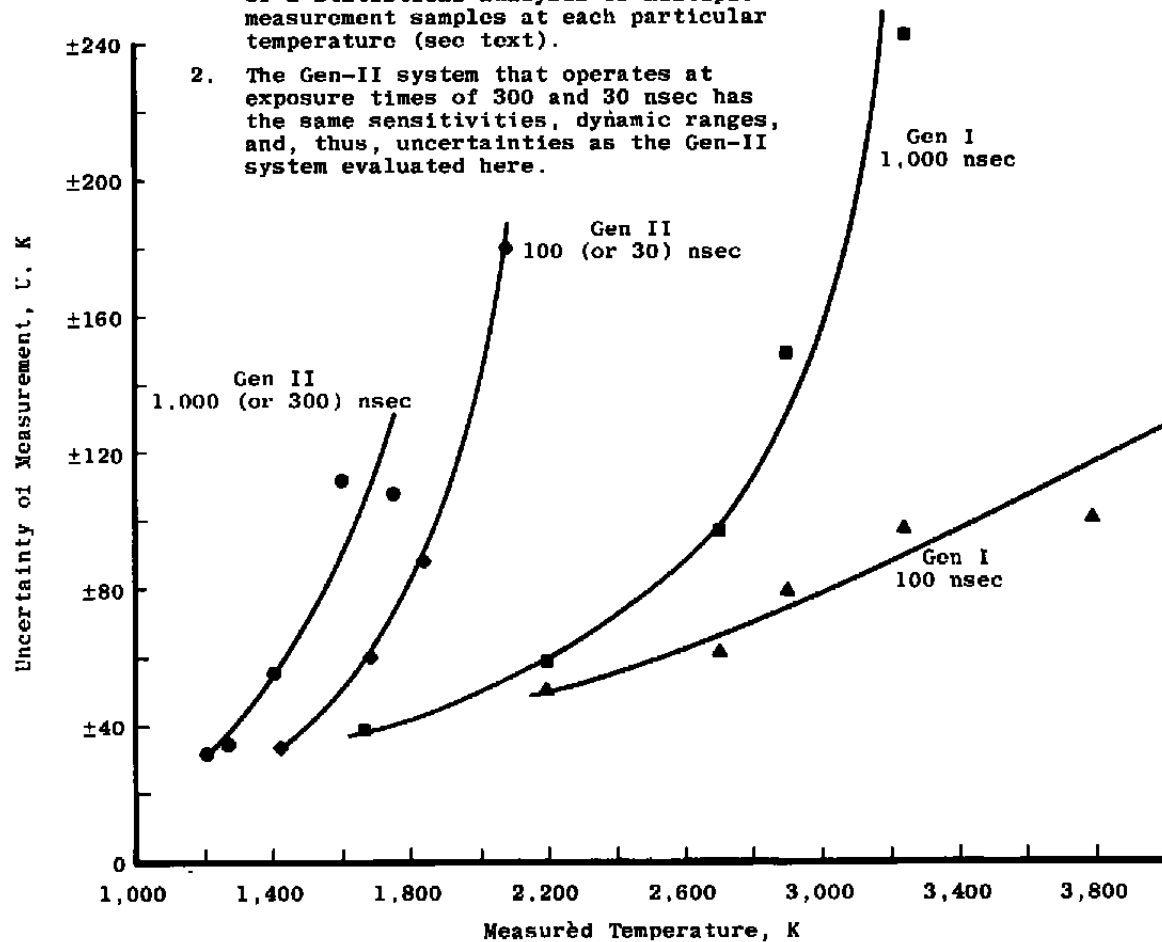


Figure 14. Photopyrometer system temperature measurement uncertainty.

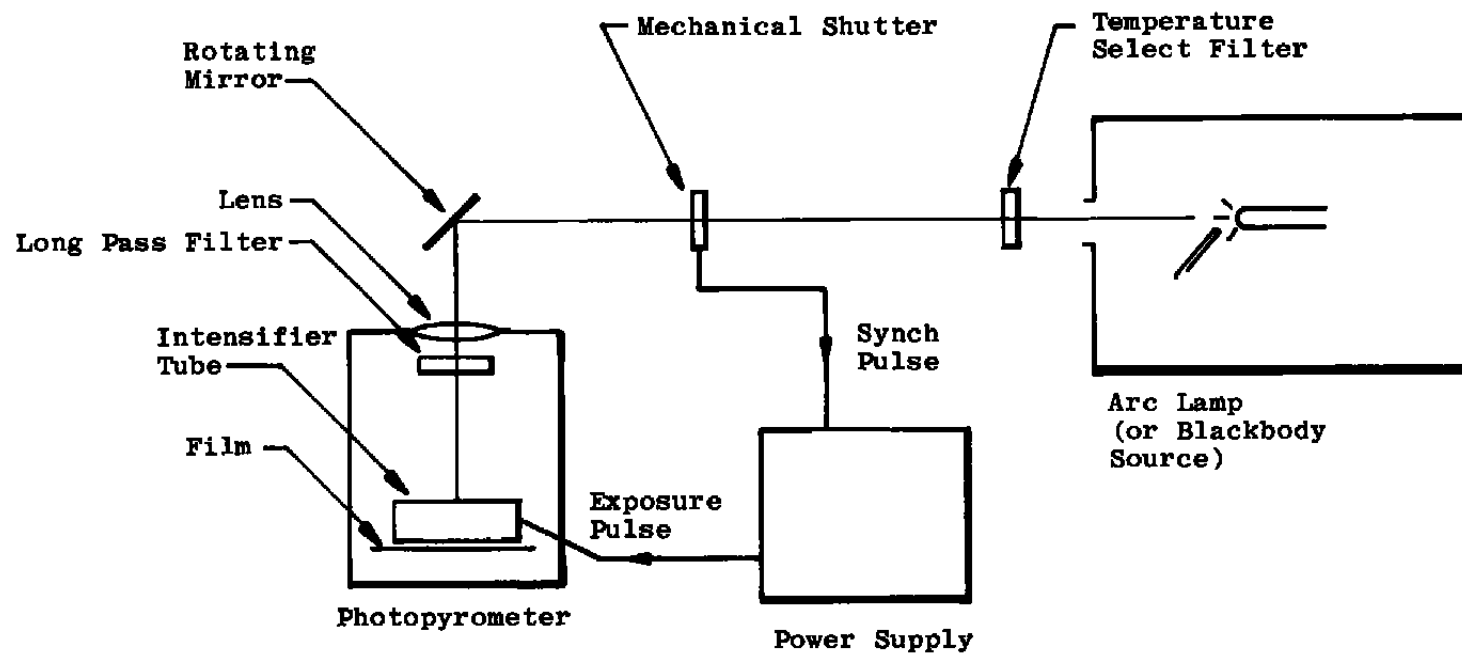
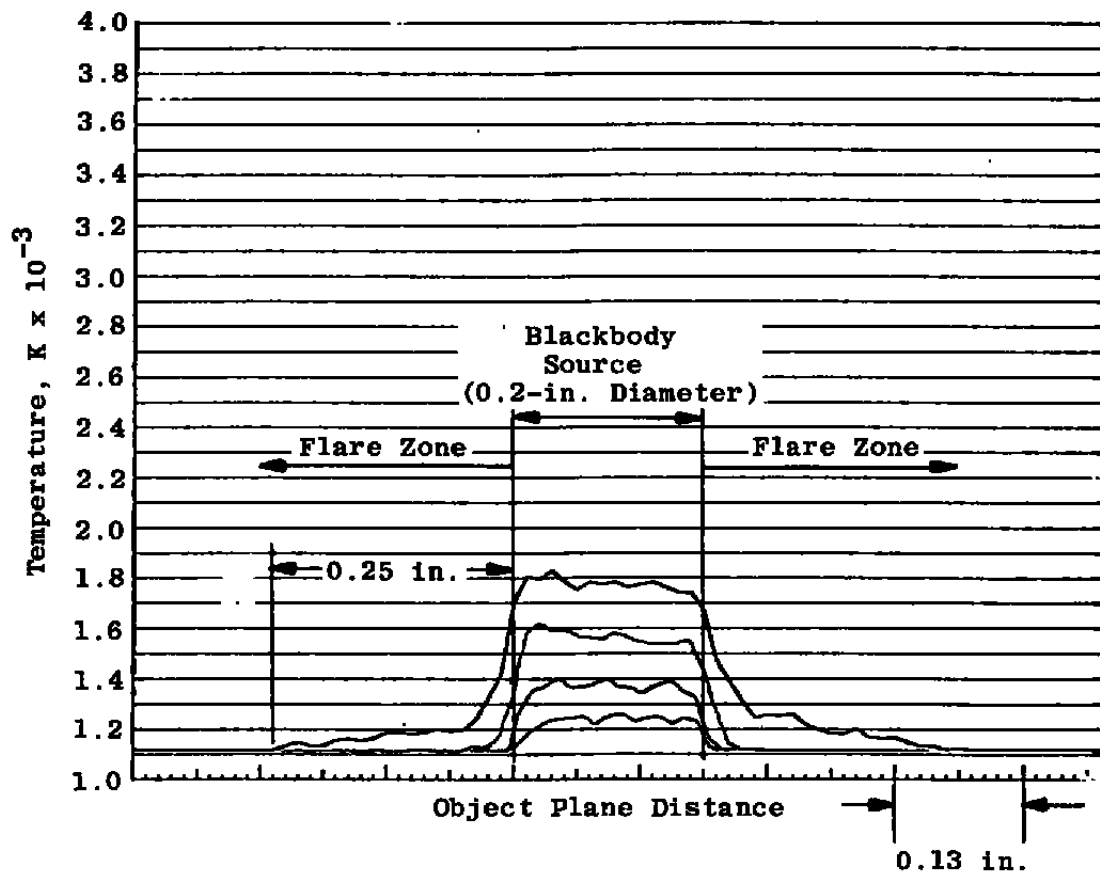
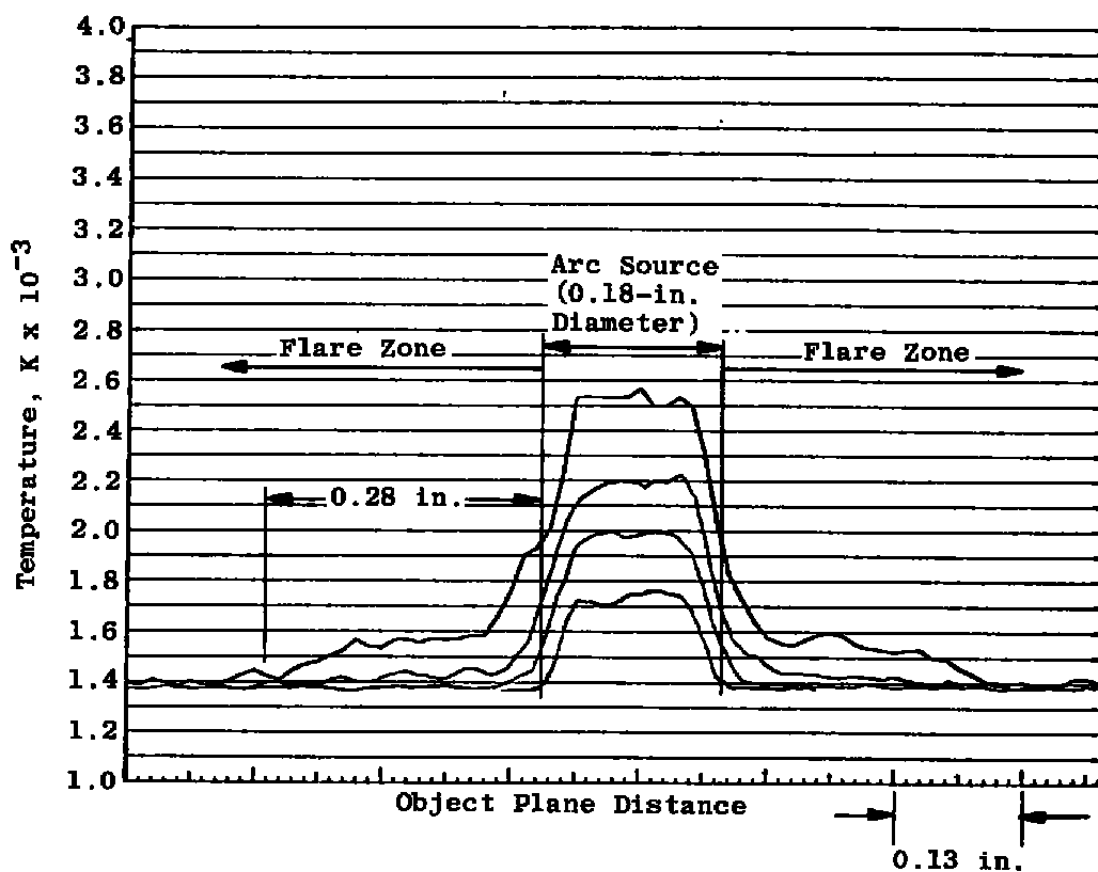


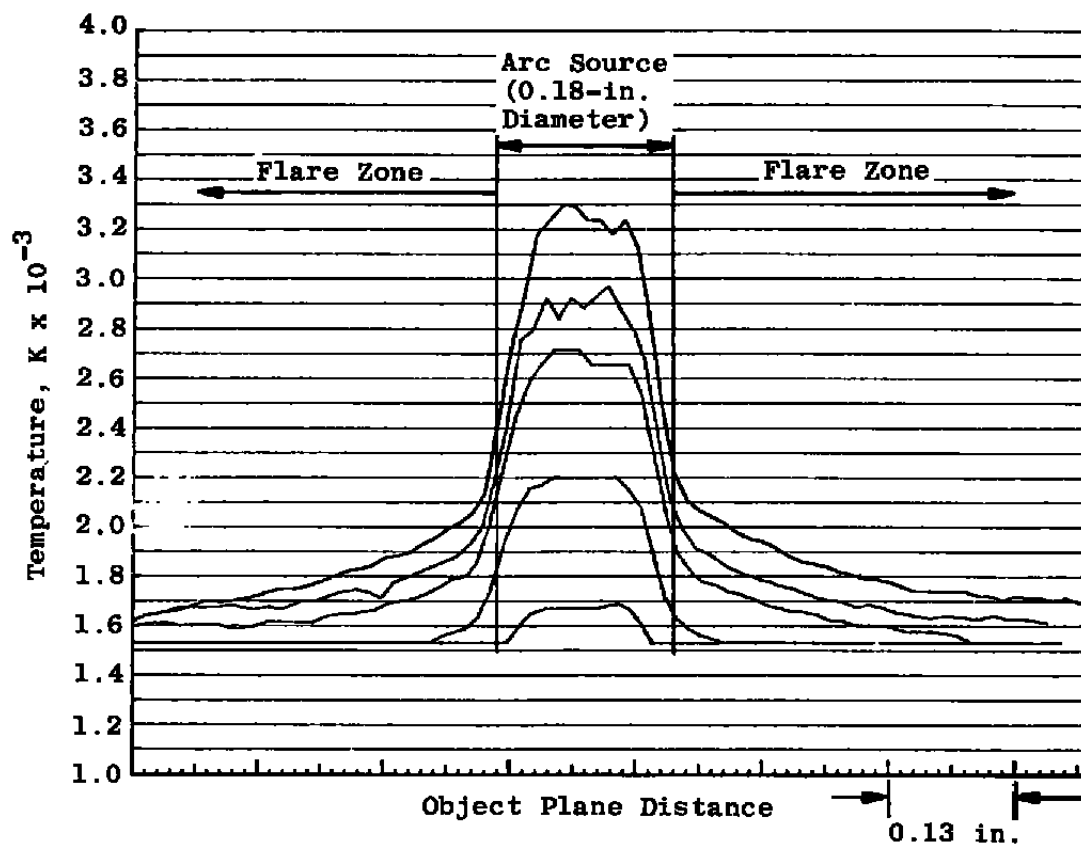
Figure 15. Flare exposure test setup.



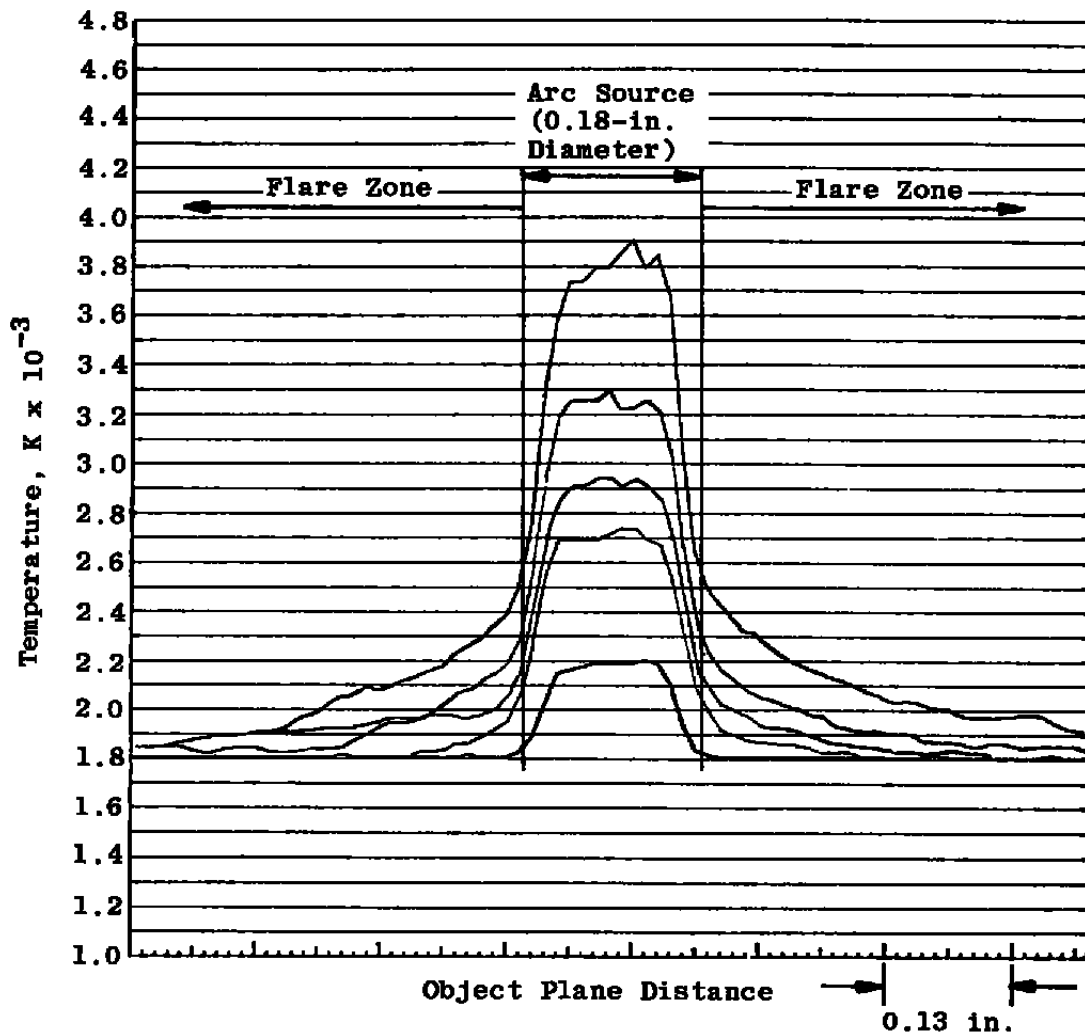
a. Gen-II photopyrometer—300-nsec (or 1,000-nsec) exposure
 Figure 16. Temperature scans—flare effects test results.



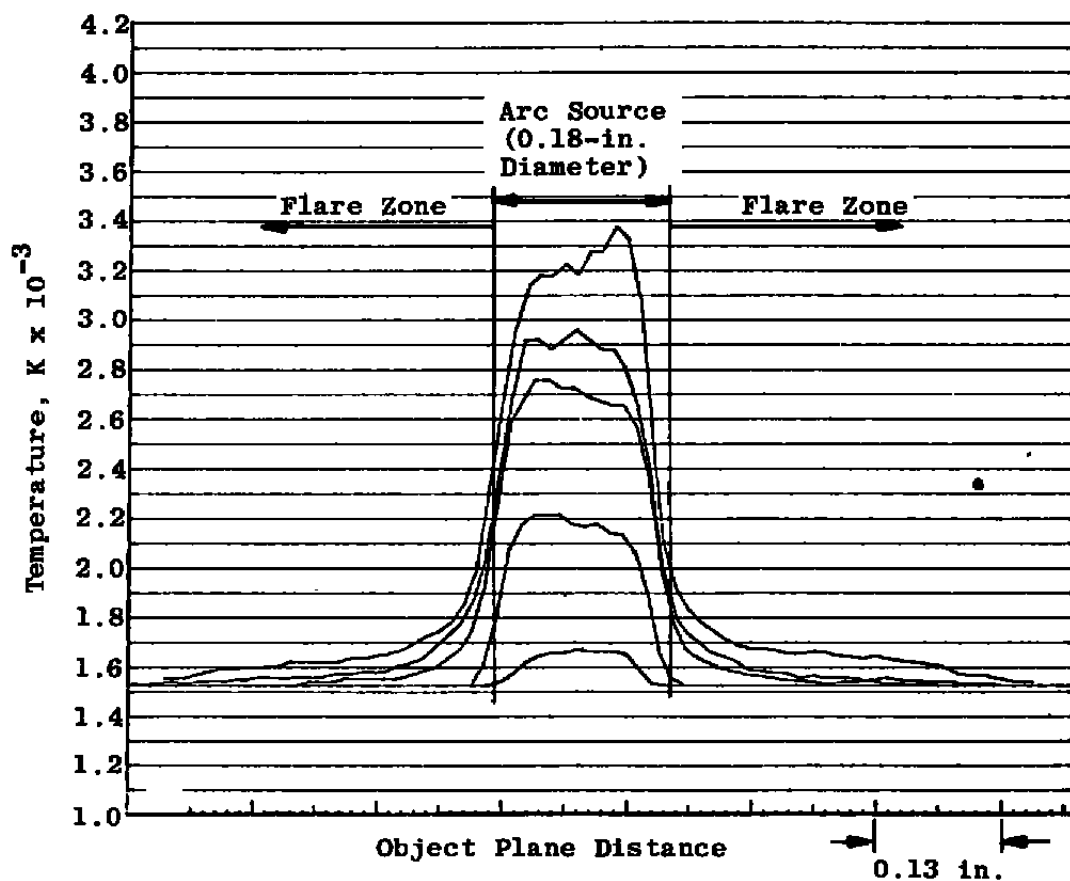
b. Gen-II photopyrometer—30-nsec (or 100-nsec) exposure
Figure 16. Continued.



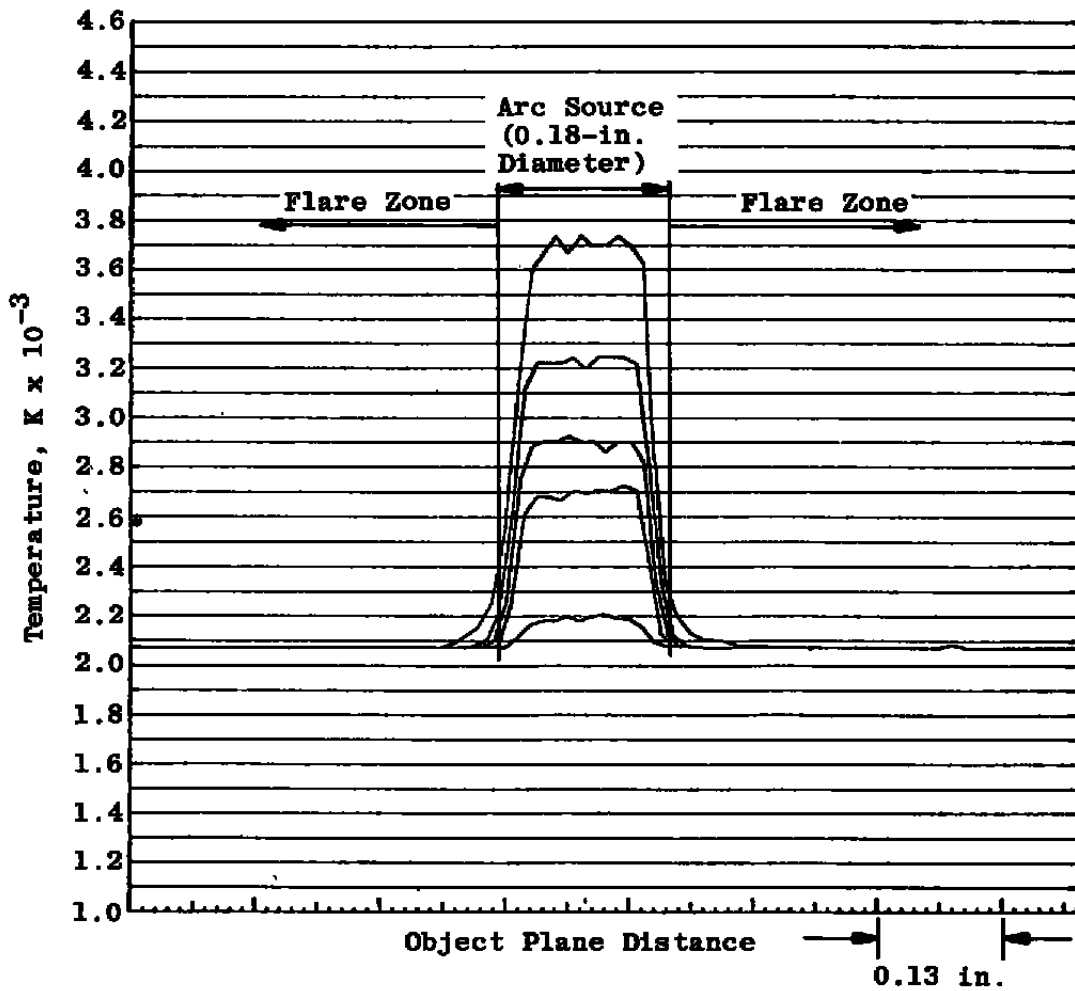
c. Standard Gen-I photopyrometer—1,000-nsec exposure
Figure 16. Continued.



d. Standard Gen-I photopyrometer—100-nsec exposure
Figure 16. Continued.



a. Low-flare Gen-I photopyrometer—1,000-nsec exposure
Figure 16. Continued.



f. Low-flare Gen-I photopyrometer—100-nsec exposure
Figure 16. Concluded.

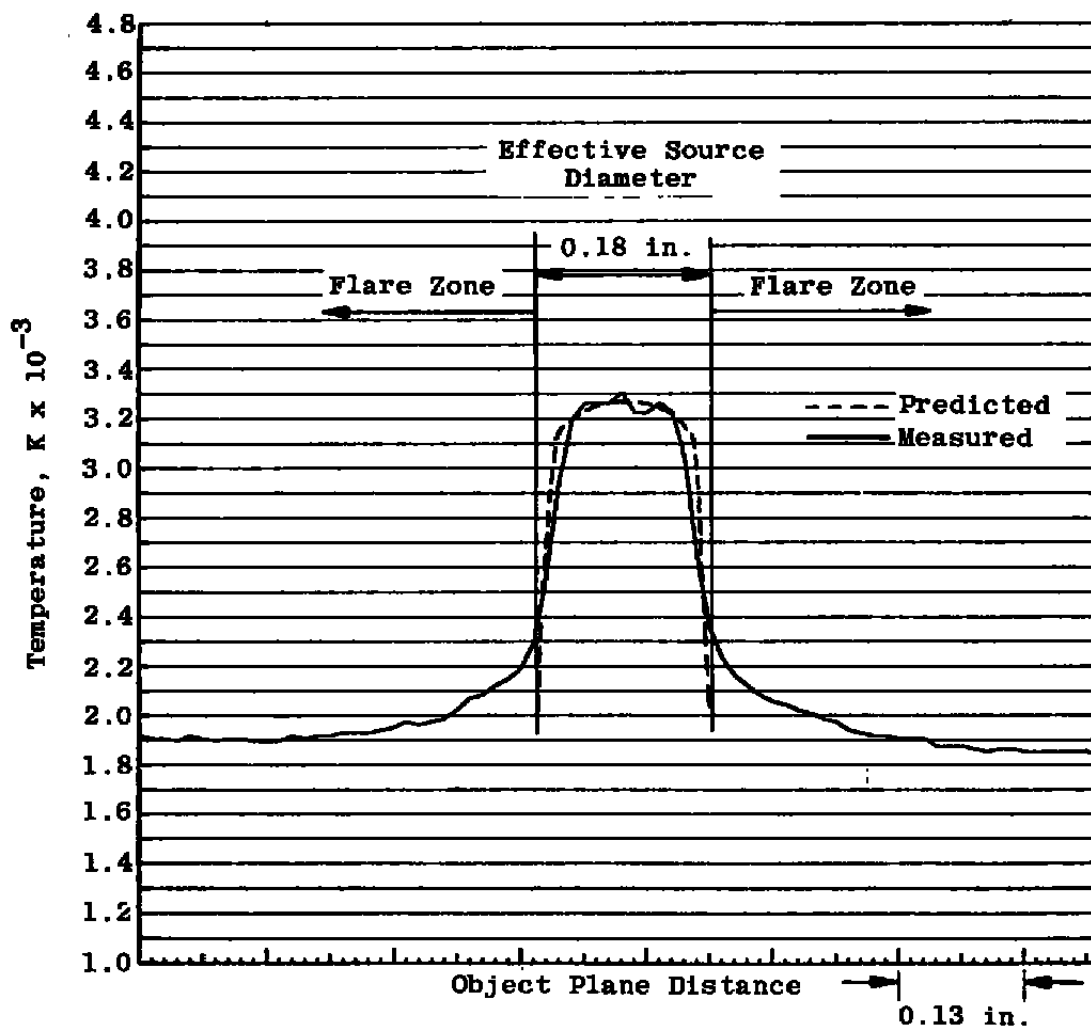


Figure 17. Predicted and measured graphite-arc lamp temperature profiles.

**Table 1. High-Speed Image Intensifier/High-Speed Photopyrometer
State-of-the-Art History**

Time Period	Pertinent Intensifier Characteristics*	Photopyrometer Lower Measurement Limit	Remarks
1970	S-11 spectral response (0.35-0.65 μm), relay lens transfer of intensified image to film	2,800 K	Initial systems
1971	S-11 spectral response, direct coupling of image to film via fiber optics faceplate	2,300 K	Improved light efficiency
1974	S-20R spectral response (0.35-0.93 μm), fiber optics coupled [†]	1,900 K	Good near-infrared response
1975	S-20R spectral response, fiber-optics coupled [†]	1,600 K	Improved version having higher gain, better near-infrared response
1976	S-20R spectral response, channel intensifier section, fiber-optics coupled ^{††}	1,250 K	Extremely high gain

*The aeroballistic range/track application requires that the general intensifier type be a proximity-focused diode, gateable at exposure times of 100 nsec or less.

[†]Type designation: Generation I (Gen-I)

^{††}Type designation: Generation II (Gen-II)

Table 2. Measurement Ranges for Track G Photopyrometers

System Type	Number Available	Exposure Duration (nsec)	Dynamic* Range (K)	Calibration Source
Gen-I Low-Flare	2	1,000 100	1,600 - 3,300 2,100 - 4,000 [†]	Graphite Arc
Gen-I Standard	1	1,000 100	1,700 - 3,400 1,950 - 4,000 [†]	Graphite Arc
Gen-II	1	1,000 100	1,250 - 1,900 1,500 - 2,400	Blackbody Blackbody and Graphite Arc
Gen-II**	1	300 30	1,250 - 1,900 1,500 - 2,400	Blackbody Blackbody and Graphite Arc

*The dynamic range lower limit is defined at signal level twice that of background noise. Values given are for f/11 lens aperture.

**This system can be operated at shorter exposure times than the other Gen-II system and still produce equivalent temperature measurement sensitivities and dynamic ranges because of the use of an especially high-gain microchannel intensifier.

[†]The upper limit is not well established; the calibration source above 3790 K is not available.

Table 3. Photographic Characteristics of Track G Photopyrometers

Objective Lens Focal Length	210 mm			
Operating Aperture	f/11			
Magnification	0.3			
Depth of Field	±0.25 in.			
Object-Plane Resolvability*	0.006 in.			
Exposure Times	30 nsec	100 nsec	300 nsec	1,000 nsec
Motion Blur (Object Plane) for Model Velocity of 15,000 ft/sec**	0.0005 in.	0.0016 in.	0.0047 in.	0.0157 in.

*"Object-plane resolvability" refers to the minimum distance between two points on the object that allows these points to be resolved unambiguously in the image. This resolvability is a characteristic of the optical system and does not include motion-blur effects that result from the imaging of moving objects.

** Viewing angle is 5 deg from head-on to model.

APPENDIX A IMAGE INTENSIFIERS

Two types of image intensifiers are currently used in Track G photopyrometers: Gen-I and Gen-II. The Gen-II devices represent state-of-the-art image intensifiers that are in production and commercially available. (More advanced, Gen-III devices are now in development.) Both intensifier types have S-20R spectral response (i.e., they respond to light at wavelengths within the 0.35- to 0.93- μm spectral region). These devices can be gated for exposure times as short as 10 nsec.

All of the image intensifiers used in Track G photopyrometers are the proximity-focused type. "Proximity" refers to the close spacing between the photocathode and anode phosphor screen. The basic proximity-focused, image intensifier diode is illustrated in Fig. A-1. An illuminated (or luminous) object is imaged onto the input face or photocathode of the image intensifier. For each point on the photocathode where photons are incident, low-energy photoelectrons are released from the surface. Energy is imparted to these electrons by accelerating them with high voltage across the small gap between the cathode and anode. After the electrons cross the small gap, they impinge on the phosphor screen where reversion to light occurs. Because of the small gap (short path), the electrons have little chance to disperse and cause defocusing.

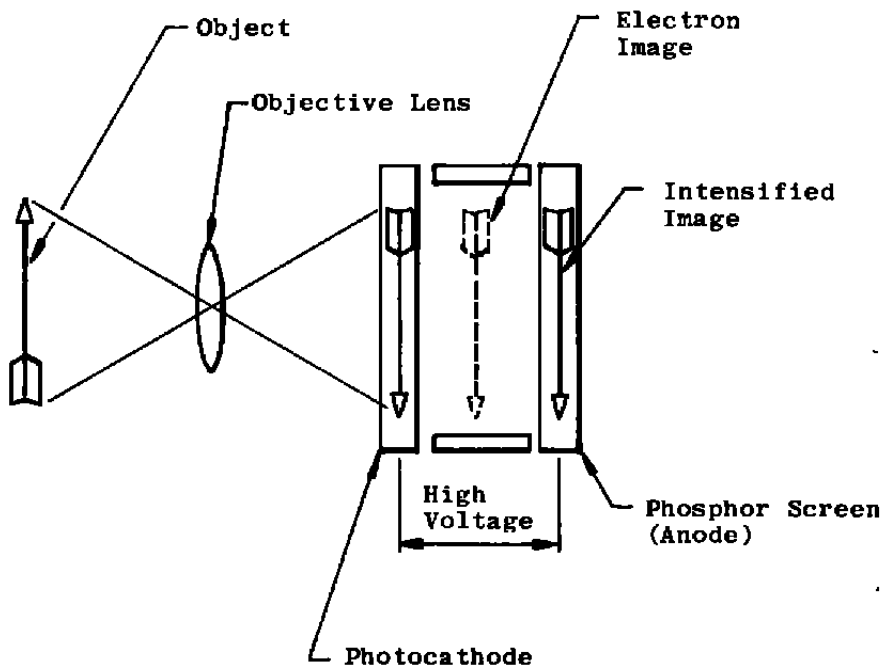


Figure A-1. Basic proximity-focused image intensifier.

A Gen-I image intensifier is shown schematically in Fig. A-2. This device uses a proximity-focused intensifier as shown in Fig. A-1 and features a fiber optics faceplate for direct and efficient transfer of the intensified image to the recording film. Gating is achieved by applying a high-voltage pulse across the photocathode-phosphor gap. The duration of this pulse, of course, defines the exposure time for the system.

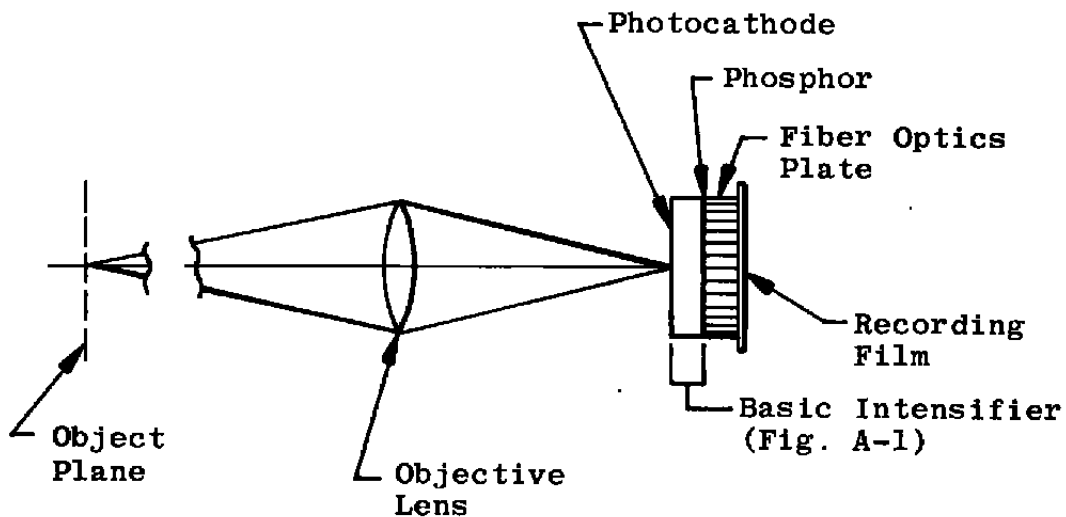


Figure A-2. Generation-I image intensifier camera system.

A schematic diagram of a Gen-II image intensifier system is shown in Fig. A-3. This system uses a microchannel electron multiplier plate between the photocathode and phosphor anode to produce higher gain (greater intensification) than the Gen-I system.

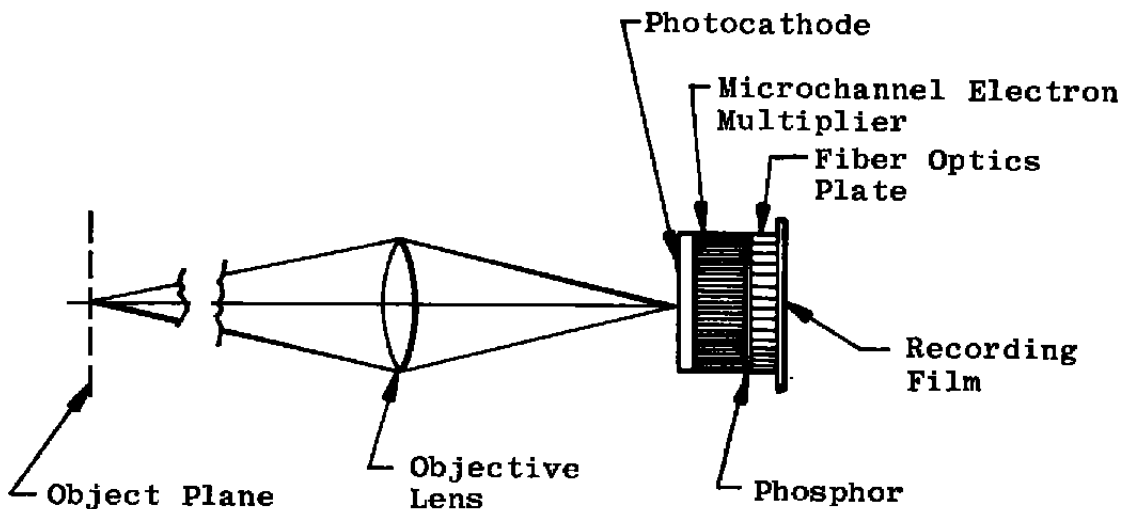


Figure A-3. Generation-II image intensifier camera system.

As with the Gen-I system, the optical image is converted to an electron image at the photocathode. The proximity of the photocathode and channel electron multiplier plate minimizes dispersion of the electron stream. Hence a minimum degradation of resolution results. An applied potential of a few hundred volts assists in the electron beam collimation and provides sufficient energy to the electrons such that the first impact of an electron in a channel of the electron multiplier yields a suitable number of secondary electrons. With potential of approximately 600 v across the channel multiplier, the secondary electrons are accelerated down the channels, cascading, multiplying, and yielding an increased number of electrons at the output face of the channel multiplier. This increased number of electrons is then further collimated and energized by a potential between the channel multiplier and phosphor anode. A fiber-optics section transfers the visible image from the phosphor to the recording film.

The main feature of the Gen-II image intensifiers, the microchannel electron multiplier plate, is comprised of millions of very small individual glass tubes or channels that have been specially treated to produce secondary electrons. Another feature that characterizes Gen-II systems is the use of three separate voltages (potential differences): (1) voltage 1, from photocathode to microchannel plate (typically 200 v); (2) voltage 2, across the microchannel plate (typically 600 v); and (3) voltage 3, from microchannel plate to phosphor anode (typically 5 kv). Gen-I systems use only one voltage—the gateable voltage from photocathode to phosphor anode. However, for the Gen-II systems, gating is achieved by switching only one of the voltages—voltage 1. The other two voltages are always applied during operation of the system.

APPENDIX B

IMAGE SPREADING EFFECTS

Intensifiers used in Track-G photopyrometers exhibit good imaging qualities over a fairly wide range of object brightness levels. However, problems are encountered when very bright objects are viewed; certain inherent intensifier characteristics combine to "spread" a bright image beyond its expected geometric boundaries. "Flare" and "halo" are two of the more common terms used by intensifier manufacturers and users to describe this effect. The bright, 3,236 K calibration spot shown in Fig. 2a is an example of an image with flare.

Image flare is attributable primarily to two possible occurrences within the image intensifier:

1. light reflections.
2. phosphor adjacency effects.

For the case at hand, internal light reflections are the stronger contributors to image spreading, or flare. The S-20R photocathodes used (Appendix A) are semitransparent; most of the light incident on this type of photocathode is transmitted directly through to the inside of the intensifier tube. Internal reflections are particularly bad within a standard, Gen-I intensifier (Figs. A-1 and A-2 of Appendix A). In these devices, the face of the phosphor nearest the photocathode is covered by a reflective aluminized coating that can redirect a high percentage of the light that originally entered through the photocathode and cause it to impinge onto the "back side" of the photocathode. Certainly, if the intensity level of this internally reflected light is high enough, this second pass through the photocathode will generate photoelectrons. These electrons will be accelerated by the high voltage, strike the phosphor, and contribute to the final image recorded.

In low-flare, Gen-I tubes, the reflective surface mentioned above is covered with an antireflective (black) coating that reduces considerably the amount of light internally reflected back onto the photocathode. The superior imaging characteristics of low-flare systems are discussed and illustrated in Sections 4.0 and 6.2.

Gen-II intensifiers are also susceptible to image flare. Light entering the tube through the semitransparent, S-20R photocathode strikes the input face of the channel electron multiplier (Fig. A-3). This surface can reflect light back onto the photocathode. Manufacturers are investigating techniques that might be used to reduce the internal reflections in Gen-II intensifiers. It is unfortunate that an antireflective coating of the

type used in improving Gen-I intensifiers cannot be used in a similar manner on the face of the channel electron multiplier. The coating used in the Gen-I case is electrically nonconductive; the Gen-II case requires that the coating be a conductor.

Phosphor adjacency effects can contribute significantly to flare around very bright images. The phosphor screens (Appendix A) used in both Gen-I and Gen-II intensifiers consist of clusters of sensitive particles supported in inert binders. Light is emitted isotropically from a cluster or cluster group upon excitation by electrons. Some of this light is scattered by adjacent (unactivated) clusters within the phosphor layer, resulting in image spreading. The severity and extent of this image spreading are, of course, a function of the intensity of the primary image.

Methods for minimizing the inherent light scattering within phosphor screens are under investigation by at least one image intensifier manufacturer; however, intensifiers with significantly improved phosphor screens are not expected to be commercially available in the near future.

Some other possible contributors to image spreading, or image anomalies in general, were investigated and were found to be of no consequence. Classical adjacency effects associated with the photographic film (light scattering within the photographic emulsion) were experimentally examined; no effects of this nature were discernible. Photopyrometer systems were designed in such a manner as to minimize internal reflections within the camera housing and between optical components. Experiments verified that no image deterioration is caused by such reflections.